medium changes at day 7 and 14. Peripheral blood monocytes were cultured in LI90-conditioned medium containing 1 μg/ml anti-human GM-CSF antibody (R&D Systems) or control IgG for 21 days. At day 7 and 14, a half medium was changed to the fresh medium.

RT-PCR

Total RNA was extracted using an RNeasy Kit (Qiagen, Tokyo, Japan). cDNAs were synthesized with 100 ng total RNA by using Superscript II and oligo (dT) primers (Invitrogen) according to the manufacturer's instruction. The resulting cDNA was amplified with AmpliTaq Gold (Applied Biosystems, Branchburg, NJ, USA) under the following conditions: for human glyceraldehyde-3-phosphate dehydrogenase (Gapdh) (5'-TGAAGGTGCGTGTGAACGGATTTGGC, 5'-TGTTGGGGGCCGAGTTGGGATA), at 95°C for 4 min followed by 30 cycles at 95°C for 30 sec, 60°C for 30 sec and 72°C for 25 sec; for human CD83 (5'-TCAAGTTATTGGAGGGTGGTG, 5'-GAGAAAAGCTCGTTCCATGC), at 95°C for 4 min followed by 33 cycles at 95°C for 30 sec, 60°C for 30 sec and 72°C for 25 sec; for human DC derived C-C chemokine (DC-CK1) (5'-GCCAGGTGTCATCCTCCTAA, 5'-GGCACAATGTCTGCTGAGAA), at 95°C for 4 min followed by 35 cycles at 95°C for 30 sec, 55°C for 30 sec and 72°C for 30 sec. For rat Gapdh (5'-CCAATGTATCCGTTGTGGAT, 5'-GTCTGGGATGGAATTGTGAG) at 95°C for 4 min followed by 25 cycles at 95°C for 30 sec, 58°C for 30 sec and 72°C for 30 sec; for rat GM-CSF (5'-GCTCACCCAACCCTGTCAC, 5'-CTCATTTCTGGACCGGCTTC) at 95°C for 4 min followed by 35 cycles at 95°C for 30 sec, 62°C for 30 sec and 72°C for 30 sec. The amplified PCR products were separated by electrophoresis on 1.5% agarose gels and stained with ethidium bromide.

Immunocytochemistry

The cultured UCB cells were fixed with 80% acetone at -20°C for 10 min and washed three times with PBS. Endogenous peroxidase was inactivated with 3% H_2O_2. The cells were incubated for 1 h with anti-human α-SMA monoclonal antibody conjugated with horseradish peroxidase (DAKO EPOS kit; clone 1A4, DAKO, Kyoto, Japan), and then washed three times with PBS. The signal was detected using 3,3'-diaminobenzidine tetrahydrochloride (DAB) liquid system (DAKO) according to the manufacturer's instruction. For analysis of CD83, the cells were incubated for 1 h with anti-human CD83 antibody conjugated with FITC (1:50; clone HB15e, Ancell, Bayport, MN, USA). The cells were washed three times with PBS and observed under a fluorescence microscope. The cells were fixed with 4% paraformaldehyde/PBS at room temperature for 20min and washed three times with PBS. Then they were blooked with 5% donkey serum containing 0.2% bovine serum albumin at room temperature for 30min and washed three times with PBS. The cells were incubated for 1 h with anti-human CD83 antibody (1:100; clone HB15e, R&D system) or anti-human DC-SIGN (CD209) antibody (1:100; R&D system). Then the cells were incubated with mouse IgG conjugated with Alexa-Fluor 488.

Mixed leukocyte reaction

Allogeneic mixed leukocyte reaction was performed as previously described.[22] T cells were isolated from adult mononuclear cells by a T cell negative isolation kit according to the manufacturer's instruction (DYNAL, Oslo, Norway). Allogeneic adult T cells (1 x 10^5 responder cells/well) were cultured in triplicate in flat-bottom 96-well plates (Greiner, Nutingen, Germany) with different number of stimulator cells (DC: T cell ratio of 1:320-1:5) pretreated with mitomycin-C. Cultures were maintained in RPMI-1640 (Sigma) supplemented with 10% FBS. To the well containing 200 μl medium, 20 μl of 100 μM 5'-bromo-2'-deoxyuridine (BrdU) was added 18 h before the end of a 5-day culture, and its incorporation was then determined with BrdU kit (Roche Diagnostics, Mannheim, Germany).

Cytokine array

Human cytokine array membranes were purchased from RayBiotech, Inc. (Norcross, GA, USA). Human cytokine array 3 was used according to the manufacturer's direction. We assayed 42 cytokines in conditioned medium that was collected after LI90 cells cultured with or without the cytokine cocktail for 21 days.

Enzyme-linked immunosorbent assay (ELISA) for GM-CSF

Measurement of GM-CSF in the medium of LI90 culture was performed by using AN'ALYZA Immunoassay System (GT, Minneapolis, MN, USA) as the manufacturer's protocol. LI90 cells were cultured in 6-well plates at a density of 4 x 10^4 cells/well for 21 days in the several culture systems. Medium was changed at day 7 and 14. Supernatants were collected at day 7, 14 and 21 of culture. Determination of GM-CSF concentration was performed in triplicate.

Coculture of UCB cells with primary HSCs

Male Wistar rats (220-300g body weight) were used. All experiments were performed according to the standard guidelines for animal experiments of the Tokyo Medical and Dental University. Rats were subjected to intraperitoneal injection of 1.5 ml CCl_4/kg body weight (Wako Pure Chemical Industries, Osaka, Japan).[23] HSCs were isolated from normal or CCl_4-damaged livers.[24] Briefly, normal or damaged livers were perfused for 10 min with SC-1 solution consisting of 8 mg/ml NaCl, 0.4 mg/ml KCl, 0.088 mg/ml $NaH_2PO_4 \cdot 2H_2O$, 0.12 mg/ml Na_2HPO_4, 2.38 mg/ml Hepes, 0.35 mg/ml $NaHCO_3$, 0.19 mg/ml EGTA and 0.9 mg/ml glucose (pH 7.3), followed by digestion at 37°C for 40 min with 0.1% pronase E (Merck, Whitehouse Station, NJ, USA) and 0.04% collagenase (Wako Pure Chemical Industries) dissolved in SC-1 solution containing 0.56 mg/ml $CaCl_2 \cdot 2H_2O$ instead of 0.19 mg/ml EGTA and 0.9 mg/ml glucose (SC-2 solution). The digested liver was excised, cut into small pieces, and incubated in SC-2 solution containing 0.08% pronase E, 0.08% collagenase and 20 μg/ml DNase I (Roche). The resulting suspension was filtered through a 150-μm steel mesh and centrifuged on an 8.2% Nycodenz™ (Axis-Shield, Oslo, Norway) cushion, which produced an HSC-enriched fraction in the upper whitish layer. The cells were washed, suspended in DMEM supplemented with 10% FBS, 70 μg/ml penicillin, and 100 μg/ml streptomycin, and plated on plastic culture dishes. Cell purity was approximately 95% as assessed by a typical star-like configuration and by detecting vitamin A autofluorescence. The resulting cells were cocultured with UCB monocytes as described above.

Results

Dendritic-shaped cells in coculture with a human HSC line

We previously reported that UCB cells differentiate into hepatocyte-like cells *in vitro*.[13] To test whether HSCs further contribute to hepatic differentiation of UCB cells, we cocultured UCB cells with the human HSC line LI90 using a cell-culture insert in a medium supplemented with the hepatocyte-inducing cytokines containing FGF-1, FGF-2, LIF, SCF and HGF as illustrated in Fig. 1A. Contrary to our expectation, LI90 did not induce hepatocyte-like cells from UCB cells. Instead, dendritic-shaped cells emerged in the UCB cell population10 days after the coculture. At 21 days of culture, these cells comprised approximately 80% of the adherent UCB cell population (Fig. 1B,C). No round-shaped hepatocyte-like cells were observed under the applied coculture conditions; however, these cells were generated from the UCB cells without LI90 coculture (Fig. 1D) as previously reported.[13] Next, we tested whether monocytes isolated from UCB cells are the source of dendritic-shaped cells. When UCB monocytes were cocultured with LI90 cells on a separate insert, dendritic-shaped cells were similarly generated (Fig. 1E). The differentiation into dendritic-shaped cells was

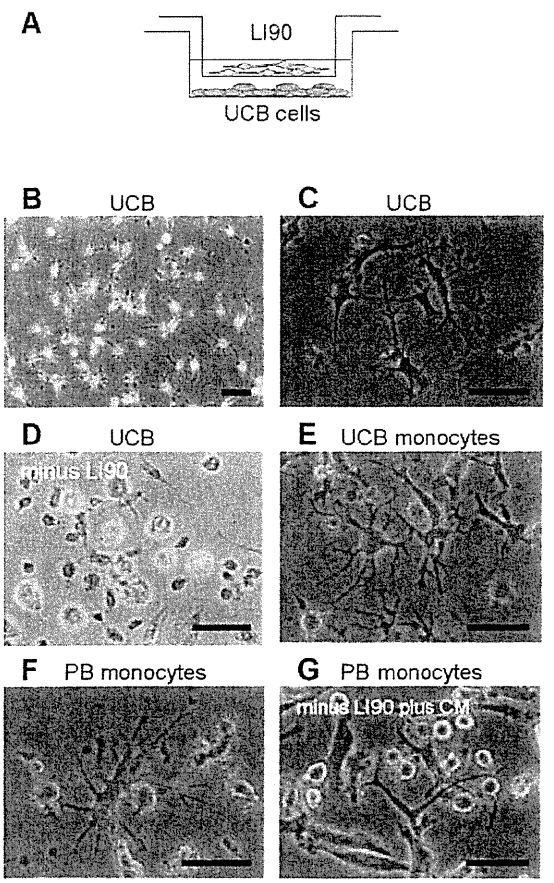

Figure 1 : Coculture of UCB and peripheral blood cells with a human stellate cell line, LI90. (A) Coculture system of UCB cells with LI90 cells. LI90 cells were seeded on the membrane of cell culture insert and human UCB-nucleated cells were seeded on the plastic well in the cytokine cocktail medium containing FGF-1, FGF-2, LIF, SCF and HGF. (B-D) Morphology of UCB-nucleated cells cocultured with (B, C) or without LI90 cells (D) in the cytokine medium for 21 days. Round-shaped cells appeared in (D). (E, F) Morphology of monocytes from UCB (UCB monocytes, E) or peripheral blood (PB monocytes, F) cocultured with LI90 in the cytokine medium for 21 days. (G) Morphology of PB monocytes cultured in the LI90 conditioned medium obtained at 14 days (CM) for 21 days. Scale bars: 100 μm (B, D); 50 μm (C, E-G).

also observed in monocytes isolated from adult peripheral blood in a coculture with LI90 (Fig. 1F). Furthermore, peripheral blood monocytes cultured in a conditioned medium of LI90 cells with the same cytokine cocktail showed morphological changes identical to those in the case of coculture mentioned above (Fig. 1G). These data show that monocytes from UCB and peripheral blood differentiated into dendritic-shaped cells in the presence of factor(s) secreted by LI90 cells in the coculture.

Characterization of dendritic-shaped cells from UCB cells cocultured with LI90 cells

We characterized whether the UCB-derived dendritic-shaped cells are functionally equivalent to DCs. LI90 cells were immunocytochemically positive for α-SMA, a marker of activated HSCs (Fig. 2A). The monocyte-derived dendritic-shaped cells were negative for α-SMA (Fig. 2B), but positive for CD83 and DC-SIGN (CD209) (Fig. 2C). RT-PCR revealed no expression of a DC-specific chemokine, DC-CK1 (CCL18),[25] in freshly isolated UCB monocytes (Fig. 2D, day 0). Upon coculturing with LI90, the UCB monocytes commence to express DC-CK1 from day 1 and the expression level gradually increased thereafter (Fig. 2D). No induction of DC-CK1 expression was seen in the UCB monocytes without LI90 coculture (data not shown). These results suggest that monocyte-derived cells induced by LI90 exhibited a DC phenotype *in vitro*.

Functional analysis of UCB-derived DCs

Next, we tested whether UCB-derived cells stimulate proliferation of T cell, a major function of DCs. After coculturing the UCB monocytes with LI90 for 21 days, the monocyte-derived cells were further cocultured with 1 x 10^5 T cells obtained from allogeneic peripheral blood and the proliferative activity of the T cells was measured by determining BrdU uptake on day 5. As shown in Fig. 2E (open circle), the monocyte-derived cells induced by LI90 coculture were capable of stimulating T-cell proliferation. The stimulating capacity was as high as that of dendritic-shaped cells cultured with TNF-α and PGE_2 for additional 2 days (Fig. 2E, closed circle). These results suggest that LI90 induces functional DCs from monocytes in the coculture condition.

Identification of factors secreted from LI90 cells in the cytokine medium

Our results indicated that factor(s) secreted by LI90 are responsible for the differentiation of monocytes into

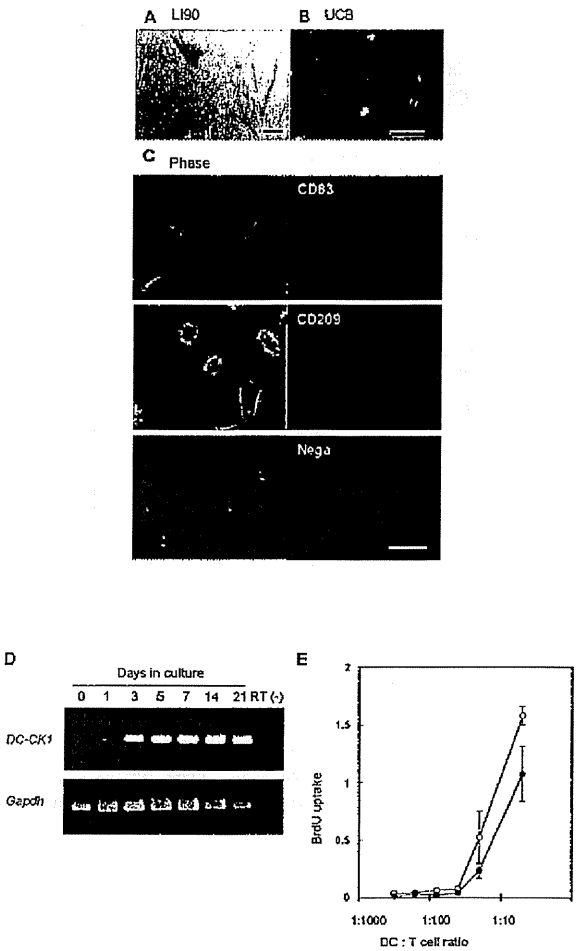

Figure 2 : Characterization of dendritic-shaped cells derived from UCB cells cocultured with LI90 cells. Immunostaining of LI90 cells (A) and UCB-derived dendritic-shaped cells (B) with anti-α-SMA antibody. Scale bars, 50 μm. (C) Immunofluorescent staining of dendritic-shaped cells with anti-CD83 or anti-CD209 antibodies. Scale bars, 50 μm. (D) RT-PCR analysis of DC-CK1 expression in dendritic-shaped cells. The RNA samples were prepared from the cultured UCB monocytes for the indicated days. No amplification was detected in a negative control (Day 21, RT-). Gapdh was used as an internal control. (E) Mixed leukocyte reaction. UCB monocytes were cocultured with LI90 for 21 days, then cultured with (closed circle) or without (open circle) 1 ng/ml PGE_2 and 25 ng/ml TNF-α for additional 2 days. The cultured cells (3.1 x 10^3-2 x 10^4 cells) were mixed with 1 x 10^5 T cells. Cell proliferation was detected by BrdU uptake.

the DC lineage in the cytokine cocktail medium. In order to identify these factor(s), we examined the factors present in the LI90 conditioned medium with and without cytokine cocktail using the Human Cytokine Protein Array System. Table 1 presents the ratio of

Table 1 : Levels of cytokines in the medium of LI90 cultured with cytokine cocktail.

fold[a]	cytokine	ratio	fold	cytokine	ratio
	GM-CSF	49.195		IL-8	1.337
	IL-1α	9.050		IL-10	1.148
	IL-1β	109.425		IL-12	2.217
>5	IL-4	5.305		Leptin	1.226
	IL-13	7.125	1-5	MCP-3	2.052
	IL-15	46.125		OSM	1.182
	MCP-2	11.792		SCF	4.068
	Ang[b]	3.298		SDF-1	1.731
	EGF	1.400		TARC	1.204
	ENA-78	3.625		TNF-α	1.235
	GCSF	1.492		TNF-β	1.691
	GRO	1.911		VEGF	1.453
	GRO-α	2.418		MCP-1	0.953
	I-309	1.150		MCSF	0.447
1-5	IFN-γ	3.473		MDC	0.134
	IGF-1	1.152	<1	MIG	0.094
	IL-2	1.736		MIP-1δ	0.134
	IL-3	1.622		PDGF-β	0.997
	IL-5	2.548		RANTES	0.614
	IL-6	1.410		TGF-β	0.843
	IL-7	1.709		Tpo	0.990

[a] Conditioned medium of LI90 without cytokine cocktails as a control. [b] Ang, angiotensin; EGF, epidermal growth factor; ENA, epithelial neutrophil-activating protein; GCSF, granulocyte-colony stimulating factor; GRO, growth-regulated oncogene; IFN-γ, interferon-γ; IGF-1, insulin-like growth factor-1; OSM, oncostatin M; SDF, stromal cell-derived factor; TARC, thymus and activation-regulated chemokine; VEGF, vascular endothelial growth factor; MCSF, macrophage-colony stimulating factor; MDC, macrophage-derived chemokine; MIG, monokine induced by gamma interferon; MIP-1δ, macrophage inflammatory protein-1δ; PDGF-β, platelet-derived growth factor-β; RANTES, regulated upon activation, normal T-cell expressed, and presumably secreted; TGF-β, transforming growth factor-β; Tpo, thrombopoietin.

cytokine production in the LI90 culture with the cytokine cocktail to without cytokine cocktail. Among the 42 cytokines assayed on the membrane, the production of 7 cytokines, including GM-CSF, IL-1α, IL-1β, IL-4, IL-13, IL-15 and MCP-2, showed more than 5-fold greater increase in the LI90 conditioned medium prepared with the cytokine cocktail medium. In particular, GM-CSF expression was drastically higher (49-fold) in the LI90 cells cultured in the cytokine medium. Since GM-CSF is known as an essential factor for inducing DC differentiation from monocytes,[3,4] we further investigated whether LI90-secreted GM-CSF directly participate DC differentiation from monocytes. When monocytes were cultured in LI90 conditioned medium with a neutralizing antibody against GM-CSF,

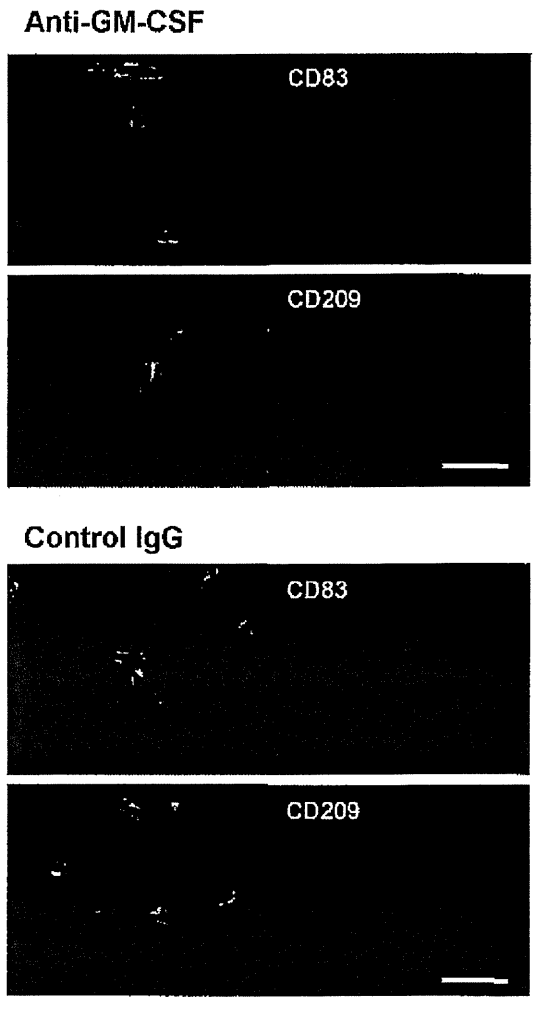

Figure 3 : Suppression of DC induction by anti-GM-CSF antibody. Monocytes from peripheral blood were cultured in the LI90 conditioned medium with anti-GM-CSF antibody or control IgG for 21 days. Immunostaining was carried out using anti-CD83 and anti-CD209 antibodies. The anti-GM-CSF antibody suppresses the expression of CD83 and DC-SIGN (CD209). Scale bars, 50 μm.

they did not change their morphology to dendritic-shaped and no induction of DC markers such as CD83 and CD209 were observed (Fig. 3). The control IgG did not suppress the expression of DC markers. Thus, GM-CSF secreted from LI90 is critical for induction of DCs from monocytes.

FGF-2 induces GM-CSF secretion in LI90

We measured the time-dependent secretion of GM-CSF from LI90 cells in the presence of the cytokine cocktail by ELISA. The concentration of GM-CSF in the

LI90-conditioned medium was 2.5 ng/ml at 14 days, and increased to 7.8 ng/ml at 21 days (Fig. 4A). On the other hand, GM-CSF was less detectable in the LI90 medium without the cytokine cocktail, suggesting that the cocktail induces expression of GM-CSF in LI90.

To identify the key cytokine involved in GM-CSF secretion from LI90 cells, we cultured LI90 cells in several combinations of FGF-1, FGF-2, LIF, SCF and HGF in the cytokine cocktail. When the LI90 cells were cultured with these 4 of the above-mentioned cytokines excluding FGF-2, GM-CSF secretion was markedly reduced similar to that when the cells were cultured without the cytokine cocktail (Fig. 4B). On the other hand, FGF-2 alone was sufficient to induce the secretion of considerable GM-CSF from LI90 cells (Fig. 4B). When UCB monocytes were cocultured with LI90 in the presence of FGF-2 alone (Fig. 4D), typical dendritic-shaped cells were observed as in addition of 5 cytokines (Fig. 4C). These results indicate that FGF-2 was the key factor responsible for GM-CSF secretion from LI90 cells, resulting in differentiation of monocytes into DCs in the LI90 coculture.

Primary HSCs are capable of inducing DC differentiation from monocytes via GM-CSF expression

To address whether HSCs are involved in DC differentiation in the liver, we examined the potential of primary HSCs to DC differentiation from monocytes. We isolated HSCs isolated from normal rat liver and similarly cocultured with human UCB monocytes. After 7 days of coculture, typical dendritic-shaped cells were barely noted (Fig. 5A). In contrast, when monocytes were cocultured with HSCs isolated from CCl_4-treated rat liver, they differentiated into dendritic-shaped cells (Fig. 5B). In fact, these monocyte-derived cells strongly expressed DC-CK1, compared to coculture with quiescent HSCs from normal liver (Fig. 5C). GM-CSF expression was high in the cultured HSCs isolated from CCl_4-treated rat liver (activated rHSC, Fig. 5D). No expression of DC-CK1 was observed in freshly isolated UCB monocytes (see Day 0 in Fig. 2D). These results imply that activated HSCs, but not quiescent HSCs, are capable of inducing DC differentiation from monocytes via GM-CSF secretion.

Discussion

In the present study, we show that HSCs induce differentiation of DCs from monocytes *in vitro*. The trans-well culture system enabled us to determine

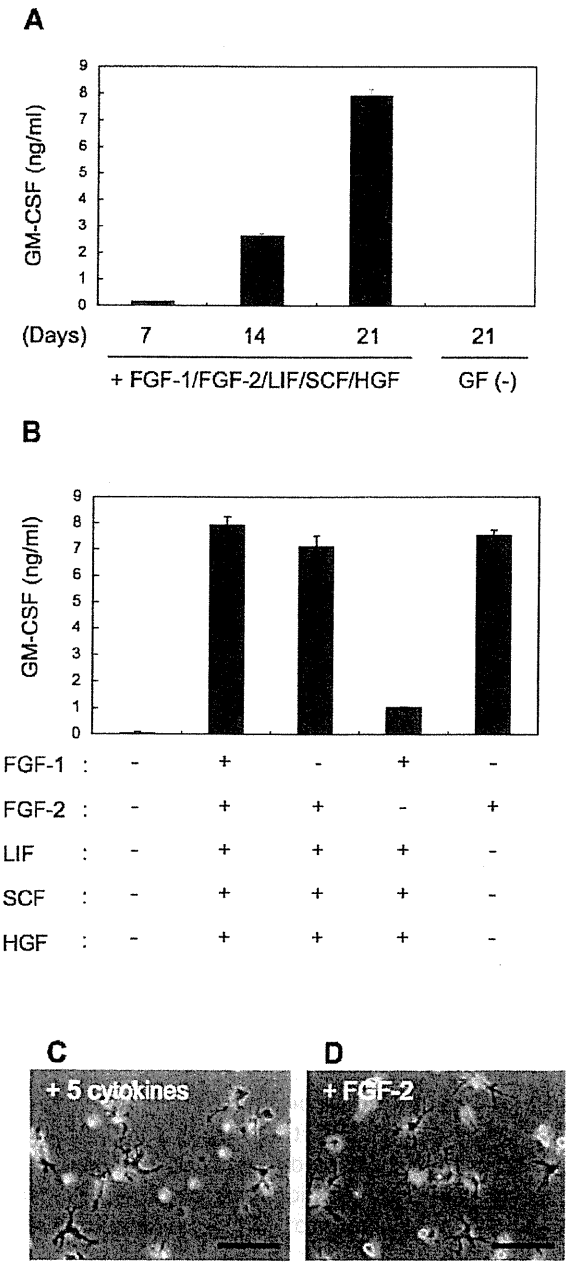

Figure 4 : GM-CSF production of LI90 cells in the cytokine medium. (A) The time course of GM-CSF production of LI90 cells ELISA was performed to detect GM-CSF in the LI90-cultured medium with or without FGF-1, FGF-2, LIF, SCF and HGF at the indicated days. GF (-), conditioned medium of LI90 cells without cytokines. (B) GM-CSF production of LI90 cells in culture with the indicated cytokines on Day 21. (C, D) Morphology of UCB monocytes cocultured with LI90 in the presence of 5 cytokines (C) or FGF-2 alone (D) for 21 days. Scale bars, 100 μm.

soluble factors from HSCs induce differentiation of monocytes to DCs. By addition of the cytokine cocktail, an HSC cell line LI90 increases the production of 7 cytokines more than 5-fold in culture. Among them, GM-CSF, IL-1β, IL-4 and IL-13 were of interest because GM-CSF and IL-4 are known to contribute to the differentiation of DCs, and IL-1β and IL-13 to their maturation [17]. It is known that GM-CSF induces DC differentiation *in vitro* from monocytes. [18] In addition, overexpression of GM-CSF in the liver results in an increase in the number of liver DCs. [19] Thus, we assume that increased secretion of GM-CSF from LI90 cells is responsible for DC differentiation from monocytes in the coculture. In fact, addition of anti-GM-CSF antibody to the LI90-conditioned medium prevented DC induction from monocytes, validating our assumption. The monocytes treated with the anti-GM-CSF neutralization antibody did not change their phenotypes and cell density, suggesting GM-CSF is not involved in survival of monocytes. We found that DCs induced by LI90 coculture from monocytes have a mature phenotype, because they exhibit a function of T cell activation. In DC differentiation *in vitro*, mature DCs are generally obtained in a 7-day culture of monocytes with GM-CSF and IL-4 followed by additional 2-day culture with maturation cytokines, such as IL-1β and IL-13. [20] Since induction of GM-CSF production from LI90 is seen over 7 days after addition of FGF2 *in vitro*, we speculate that downstream signaling pathway(s), which are activated by FGF-2 signaling, indirectly participate in GM-CSF production in LI90.

Uwatoku et al [21] reported that Kupffer cells can recruit DC precursors and DCs by direct binding to N-acetylgalactosamine-specific sugar receptors in the sinusoidal area. Furthermore, coculture of human monocytes with rat biliary epithelial cells or human non-parenchymal cells induces DC differentiation from monocytes. [22] However, it remains obscure whether HSCs are involved in DC differentiation. To examine a possible contribution of activated HSCs in an injured liver for the generation of DCs from monocytes, we cocultured monocytes with rat primary activated HSCs (Fig. 5). We found that activated HSCs isolated from CCl_4-treated rat liver markedly express GM-CSF and, thereby induce DC-CK1-expressing DCs extensively even in the xenogeneic coculture. Our results suggest that GM-CSF secreted from activated HSCs induces DC differentiation from monocytes in an injured liver.

Taking together previous reports and our present observations, we proposed a model of the generation of DCs from monocytes in an injured liver (Fig. 6). Upon

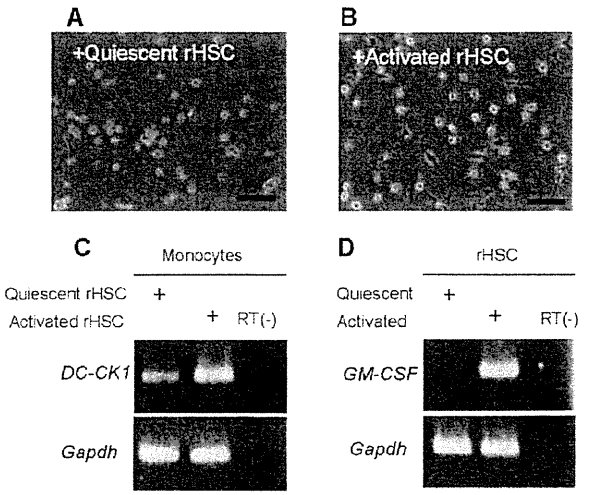

Figure 5 : Coculture of UCB monocytes with HSCs from normal and CCl_4-treated rats. (A, B) Morphology of UCB monocytes cocultured with HSCs from normal (A) or CCl_4-treated rat (B) in the cytokine medium for 7 days. Scale bars: 100 μm. (C) The gene expression of DC-CK1 in UCB monocytes cocultured with HSCs from normal (quiescent rHSC, lane 1) or CCl_4-treated rat (activated rHSC, lane 2) for 14 days. No amplification was detected in a negative control (activated rHSC, RT-). (D) The gene expression of GM-CSF in HSCs from normal (quiescent rHSC, lane 1) or CCl_4-treated rat (activated rHSC, lane 2) for 14 days under the coculture with UCB monocytes.

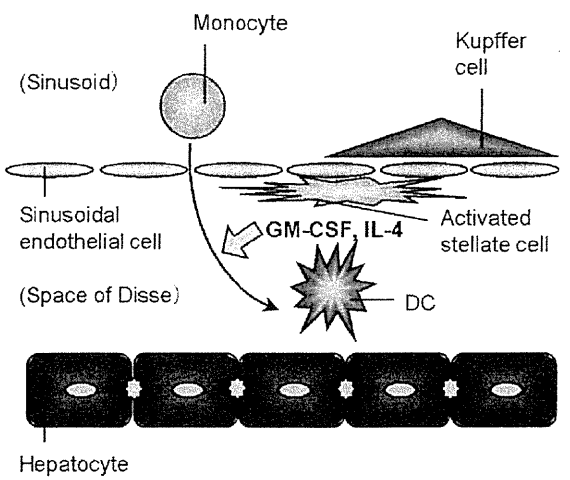

Figure 6 : A proposed model for generation of DCs in the injured liver. HSCs reside at the space of Disse in the sinusoids and in case of liver injury they are activated and release inflammatory cytokines including GM-CSF. Monocytes or dendritic precursor cells enter the space of Disse by cytokines released from several types of cells, including activated HSCs. In the space of Disse, immature DCs are induced from monocytes or dendritic precursor cells by GM-CSF and IL-4 with subsequent maturation by other cytokines like IL-1β and IL-13 released from activated HSCs. Mature DCs will migrate to lymph nodes via Glisson's sheath.

liver injury, HSCs in the space of Disse are activated and the activated HSCs consequently produce cytokines, including GM-CSF. These cytokines may attract monocytes or DC precursors into the space of Disse and contribute to monocyte differentiation into DCs. A histological analysis showed that DCs in the space of Disse are in direct contact with HSCs.[27] With regard to immune tolerance, Yu et al.[26] reported that activated HSCs suppress T-cell proliferation. Although the role of HSCs in hepatic immune responses is not fully understood,[18] HSCs may participate in the hepatic immune system via direct or indirect cellular interaction, including DC differentiation.

We identified that, among FGF-1, FGF-2, LIF, SCF and HGF in the cytokine cocktail, FGF-2 alone is sufficient to induce GM-CSF secretion in the human HSC line LI90, subsequently resulting in DC differentiation from monocytes in culture. Currently, 23 FGF genes have been identified in mice.[29] FGFs mediate a variety of cellular responses during organ development, injury, and regeneration. FGF signaling is mediated by binding FGF to FGF receptors (FGFRs), which belong to receptor tyrosine kinases. Four FGFRs have been identified and a variety of FGFR isoforms are known to be generated by alternative splicing of their transcripts. FGF-1 binds all known FGF receptors, whereas FGF-2 binds FGFR1b, FGFR1c, FGFR2c, FGFR3c, and FGFR4. FGF-1 and FGF-2 are expressed in a variety of tissues during both development and adulthood, but they are hardly expressed in normal liver. Induced FGF-2 expression has been known in HSCs during liver regeneration, and FGF-2 acts as a mitogen in autocrine and paracrine manners.[30,31] Gene knockout studies indicate that FGF-1 does not compensate the loss of FGF-2 in embryogenesis even though both FGF-1 and FGF-2 share the receptors.[32] It remains elusive how FGF-1 and FGF-2 differently affect cell responses. Heparan sulfate is known to modulate binding activities of those ligands to FGF receptors.[33] We found that activated HSCs isolated from CCl_4-treated rat liver markedly expressed GM-CSF (Fig. 5D). It seems that autocrine FGF-2 signaling in activated HSCs or paracrine effects of FGF-2 from other cells induce HSCs to secrete GM-CSF in the injured liver. Further studies will be necessary to address whether other cytokines are involved in FGF-2-mediated GM-CSF production in HSCs.

Acknowledgements

This work was supported in part by Grants-in-Aid for Scientific Research (13470232, 16390357 and 18390343) from the Ministry of Education, Culture, Sports, Science and Technology, Japan. The authors declare no conflict of interest in this work. The authors thank Dr. K. Yasumizu (Kanto Medical Center NTT East Corporation, Tokyo, Japan) for supplying umbilical cord blood, Dr. T. Matsuura (The Jikei University School of Medicine, Tokyo, Japan) for providing the LI90 cell line, Dr. N. Kawada (Osaka City University) for preparing rat stellate cells and Dr. K. Nakahama (Tokyo Medical and Dental University) for supporting the neutralizing antibody experiment.

Reference

1. Banchereau J, Steinman RM. Dendritic cells and the control of immunity. Nature 1998; 392: 245-52.
2. Longoni D, Piemonti L, Bernasconi S, et al. Interleukin-10 increases mannose receptor expression and endocytic activity in monocyte-derived dendritic cells. Int J Clin Lab Res 1998; 28: 162-9.
3. Inaba K, Inaba M, Romani N, et al. Generation of large numbers of dendritic cells from mouse bone marrow cultures supplemented with granulocyte/macrophage colony-stimulating factor. J Exp Med 1992; 176: 1693-702.
4. Sallusto F, Lanzavecchia A. Efficient presentation of soluble antigen by cultured human dendritic cells is maintained by granulocyte/macrophage colony-stimulating factor plus interleukin 4 and downregulated by tumor necrosis factor α. J Exp Med 1994; 179: 1109-18.
5. Rieser C, Böck G, Klocker H, et al. Prostaglandin E2 and tumor necrosis factor α cooperate to activate human dendritic cells: synergistic activation of interleukin 12 production. J Exp Med 1997; 186: 1603-8.
6. Muraille E, Trez CD, Pajak B, et al. T cell-dependent maturation of dendritic cells in response to bacterial super antigens. J Immunol 2002; 168: 4352-60.
7. Lau AH, Thomson AW. Dendritic cells and immune regulation in the liver. Gut 2003; 52: 307-14.
8. Crispe IN. Hepatic T cells and liver tolerance. Nat Rev Immunol 2003; 3: 51-62.
9. Kudo S, Matsuno K, Ezaki T, et al. A novel migration pathway for rat dendritic cells from the blood: hepatic sinusoids-lymph translocation. J Exp Med 1997; 185: 777-84.
10. Sato K, Nagayama H, Tadokoro K, et al. Interleukin-13 is involved in functional maturation of human peripheral blood monocyte-derived dendritic cells. Exp Hematol 1999; 27: 326-36.
11. Cabillic F, Rougier N, Basset C, et al. Hepatic environment elicits monocyte differentiation into a dendritic cell subset directing Th2 response. J Hepatol 2006; 44: 552-9.
12. Uwatoku R, Suematsu M, Ezaki T, et al. Kupffer cell-mediated recruitment of rat dendritic cells to the liver:

roles of N-acetylgalactosamine-specific sugar receptors. Gastroenterology 2001; 121: 1460-72.
13. Wake K. Perisinusoidal stellate cells (fat-storing cells, interstitial cells, lipocytes), their related structure in and around the liver sinusoids, and vitamin A-storing cells in extrahepatic organs. Int Rev Cytol 1980; 66: 303-53.
14. Asahina K, Sato H, Yamasaki C, et al. Pleiotrophin/heparin-binding growth-associated molecule as a mitogen of rat hepatocytes and its role in regeneration and development of liver. Am J Pathol 2002; 160: 2191-205.
15. Geerts A. History, heterogeneity, developmental biology, and functions of quiescent hepatic stellate cells. Semin Liver Dis 2001; 21: 311-35.
16. Bataller R, Brenner DA. Liver fibrosis. J Clin Invest 2005; 115: 209-18.
17. Pinzani M, Marra F. Cytokine receptors and signaling in hepatic stellate cells. Semin Liver Dis. 2001; 21: 397-416.
18. Winau F, Hegasy G, Weiskirchen R, et al. Ito cells are liver-resident antigen-presenting cells for activating T cell responses. Immunity 2007; 26: 117-29.
19. Kakinuma S, Tanaka Y, Chinzei R, et al. Human umbilical cord blood as a source of transplantable hepatic progenitor cells. Stem Cells 2003; 21: 217-27.
20. Tabata N, Ito M, Shimokata K, et al. Expression of fusion regulatory proteins (FRPs) on human peripheral blood monocytes: induction of homotypic cell aggregation and formation of multinucleatd giant cells by anti-FRP-1 monoclonal antibodies. J Immunol 1994; 153: 3256-66.
21. Murakami K, Abe T, Miyazawa M, et al. Establishment of a new human cell line, LI90, exhibiting characteristics of hepatic Ito (fat-storing) cells. Lab Invest 1995; 72: 731-9.
22. Sorg RV, Andres S, Kogler G, et al. Phenotypic and functional comparison of monocytes from cord blood and granulocyte colony-stimulating factor-mobilized apheresis products. Exp Hematol 2001; 29: 1289-94.
23. Wang YQ, Ikeda K, Ikebe T, et al. Inhibition of hepatic stellate cell proliferation and activation by the semisynthetic analogue of fumagillin TNP-470 in rats. Hepatology 2000; 32: 980-9.
24. Kawada N, Tran-Thi TA, Klein H, et al. The contraction of hepatic stellate (Ito) cells stimulated with vasoactive substances. Possible involvement of endothelin 1 and nitric oxide in the regulation of the sinusoidal tonus. Eur J Biochem 1993; 213: 815-23.
25. Kusano F, Tanaka Y, Marumo F, et al. Expression of C-C chemokines is associated with portal and periportal inflammation in the liver of patients with chronic hepatitis C. Lab Invest 2000; 80: 415-22.
26. Pillarisetty VG, Miller G, Shar AB, et al. GM-CSF expands dendritic cells and their progenitors in mouse liver. Hepatology 2003; 37: 641-52.
27. Sato T, Yamamoto H, Sasaki C, et al. Maturation of rat dendritic cells during intrahepatic translocation evaluated using monoclonal antibodies and electron microscopy. Cell Tissue Res 1998; 294: 503-14.
28. Yu M-C, Chen C-H, Liang X, et al. Inhibition of T-cell responses by hepatic stellate cells via B7-H1-mediated T-cell apoptosis in mice. Hepatology 2004; 40: 1312-21.
29. Eswarakumar VP, Lax I, Schlessinger J. Cellular signaling by fibroblast growth factor receptors. Cytokine Growth Factor Rev 2005; 16: 139-49.
30. Baruch Y, Shoshany G, Neufeld G, et al. Basic fibroblast growth factor is hepatotropic for rat liver in regeneration. J Hepatol 1995; 23: 328-32.
31. Hioki O, Minemura M, Shimizu Y, et al. Expression and localization of basic fibroblast growth factor (bFGF) in the repair process of rat liver injury. J Hepatol 1996; 24: 217-24.
32. Miller D, Ortega S, Bashayan O, et al. Compensation by fibroblast growth factor 1 (FGF1) dose not account for the mild phenotypic defects observed in FGF2 null mice. Mol Cell Biol 2000; 20: 2260-8.
33. Kan M, Wu X, Wang F, et al. Specificity for fibroblast growth factors determined by heparan sulfate in a binary complex with the receptor kinase. J Biol Chem 1999; 274: 15947-52.

OPEN ACCESS Freely available online

PLoS one

Onset of Quiescence Following p53 Mediated Down-Regulation of H2AX in Normal Cells

Yuko Atsumi[1☯], Hiroaki Fujimori[1,3☯], Hirokazu Fukuda[2☯], Aki Inase[2], Keitaro Shinohe[3], Yoshiko Yoshioka[3], Mima Shikanai[3], Yosuke Ichijima[3], Junya Unno[4], Shuki Mizutani[4], Naoto Tsuchiya[2], Yoshitaka Hippo[2], Hitoshi Nakagama[2], Mitsuko Masutani[1], Hirobumi Teraoka[3], Ken-ichi Yoshioka[1,3]*

1 Division of Genome Stability Research, National Cancer Center Research Institute, Tokyo, Japan, 2 Division of Cancer Development System, National Cancer Center Research Institute, Tokyo, Japan, 3 Department of Pathological Biochemistry, Medical Research Institute, Tokyo Medical and Dental University, Tokyo, Japan, 4 Department of Pediatrics and Developmental Biology, Graduate School of Medical and Dental Sciences, Tokyo Medical and Dental University, Tokyo, Japan

Abstract

Normal cells, both *in vivo* and *in vitro*, become quiescent after serial cell proliferation. During this process, cells can develop immortality with genomic instability, although the mechanisms by which this is regulated are unclear. Here, we show that a growth-arrested cellular status is produced by the down-regulation of histone H2AX in normal cells. Normal mouse embryonic fibroblast cells preserve an H2AX diminished quiescent status through p53 regulation and stable-diploidy maintenance. However, such quiescence is abrogated under continuous growth stimulation, inducing DNA replication stress. Because DNA replication stress-associated lesions are cryptogenic and capable of mediating chromosome-bridge formation and cytokinesis failure, this results in tetraploidization. Arf/p53 module-mutation is induced during tetraploidization with the resulting H2AX recovery and immortality acquisition. Thus, although cellular homeostasis is preserved under quiescence with stable diploidy, tetraploidization induced under growth stimulation disrupts the homeostasis and triggers immortality acquisition.

Citation: Atsumi Y, Fujimori H, Fukuda H, Inase A, Shinohe K, et al. (2011) Onset of Quiescence Following p53 Mediated Down-Regulation of H2AX in Normal Cells. PLoS ONE 6(8): e23432. doi:10.1371/journal.pone.0023432

Editor: Michael Polymenis, Texas A&M University, United States of America

Received April 11, 2011; **Accepted** July 17, 2011; **Published** August 12, 2011

Funding: This study was supported by MEXT KAKENHI (20770136 and 20659047). The funders had no role in study design, data collection and analysis, decision to publish, or preparation of the manuscript.

Competing Interests: The authors have declared that no competing interests exist.

* E-mail: kyoshiok@ncc.go.jp

☯ These authors contributed equally to this work.

Introduction

Cancer is a disease associated with genomic instability and the accumulation of mutations [1]. Unlike specific chromosomal translocation-associated tumors, most cancers associated with aging develop either chromosomal instability (CIN) or microsatellite instability (MIN) [2]. While MIN is associated with mismatch repair deficiency, CIN develops even in a normal background [3]. However, the mechanisms by which CIN and MIN develop remain elusive.

A recent genomic analysis of various cancers revealed that massive genomic rearrangements, including loss of heterozygosity (LOH) and chromosomal translocation, amplification and deletion, do not gradually accumulate over time, as conventionally thought, but appear to be acquired in a single catastrophic event [4]. One of such events could be associated with tetraploidization because tetraploidy is a common early event in cancer cells with CIN [5]. Tetraploidy is observed in cells during the initial stages of cancer [6,7] as well as in precancerous stages such as dysplasia [8,9], but not in malignant cancer cells, which usually exhibit aneuploidy in association with deploidization [5]. Furthermore, analogous to changes observed in cancer genomes, the immortalization of mouse embryonic fibroblasts (MEFs) occurs with tetraploidy and mutation of the Arf/p53 module, which eventually evolves into aneuploidy during serial cultivation [10].

In the initial stages of carcinogenesis, cells are subjected to oncogenic stress, resulting in the accumulation of DNA replication stress-associated lesions and the onset of barrier responses such as senescence and apoptosis [11,12]. This effect can be reproduced *in vitro* by the activation of oncogenes [11] and accelerated growth stimulation [12] due to the induction of accelerated S-phase entry and the resulting DNA replication stress. Importantly, genomic instability is generated under these conditions [11,12] because DNA replication stress-associated lesions persist into M phase and mediate chromosomal bridge formation and cytokinesis failure, resulting in tetraploidization [10]. In fact, tetraploidization of MEFs is induced via chromosomal bridge formation prior to the onset of immortality with mutation of Arf/p53 [10], although it is still unclear how tetraploidization induces immortality. Since such tetraploidization is specifically observed during senescence, tetraploidization might be a defect that occurs during cell proliferation or growth arrest. In fact, similar to cells in the initial stages of carcinogenesis, senescent cells often accumulate irreparable DNA lesions [13,14] and frequently exhibit genomic instability [15].

The development of cancer, as well as the onset of immortality in cells *in vitro*, is tightly associated with mutations in the Arf/p53 module [16–18]. Although this is ascribed to the role of p53 in

cancer prevention, the regulation and roles of p53 are complex [18]. While constitutively active p53 mediates premature aging in mice [19–21], additional single gene copies of *Arf* and *p53* under functional regulation mediate longevity and cancer prevention [22]. Similarly, while the accumulation of p53 induces cellular senescence and apoptosis [16,17], additional single gene copies of *Arf* and *p53* in MEFs has a protective effect from immortalization [22], suggesting that they help to maintain homeostasis under undamaged conditions. This raises the questions of the identity of the regulatory target of p53 in preserving cellular homeostasis under normal conditions and how cellular homeostasis preservation and abrogation are associated with genomic status and p53 regulation.

This study focused on the mechanism by which normal cells under serial proliferation regulate homeostasis preservation and abrogation and sought to identify the regulatory target of p53. Our results illustrated two distinct conditions that could result in growth-arrested cells: (i) cells that maintain continuous quiescence by down-regulating H2AX (a variant of core histone H2A) under p53 regulation and stable-diploidy maintenance; and (ii) cells that develop tetraploidy and immortality under continuous growth stimulation, characterized by the accumulation of γH2AX foci. Thus, oncogenic stress under growth stimulation triggers catastrophic tetraploidization that leads to immortalization in association with the accompanying mutation of the Arf/p53 module and recovery of H2AX expression and growth activity.

Results

Immortality is prevented in quiescent cells that maintain genomic stability

MEFs cultured under the standard 3T3 protocol (Std-3T3) senesce in association with oxygen sensitivity [23], which is followed by the development of immortality with tetraploidy [10] and mutation of the Arf/p53 module [22], similar to the process of carcinogenesis. In addition, similar to cells in the initial stages of carcinogenesis, spontaneous DNA lesions accumulate in senescent MEFs under Std-3T3 conditions prior to the development of immortality [10], which suggests that growth stimulation induced under Std-3T3 conditions might overwhelm senescent MEFs. Therefore, MEFs under Std-3T3 conditions were compared with MEFs exposed to temporary serum deprivation (tSD-3T3), which induces occasional growth arrest (Fig. 1A). Under Std-3T3 conditions, MEFs were immortalized with tetraploidy that progresses to aneuploidy (Fig. 1A–C). On the other hand, MEFs cultured under tSD-3T3 conditions never developed immortality and preserved quiescence with stable diploidy (Fig. 1A, C). This indicates that temporal growth arrest prevents immortalization and supports genomic stability. Conversely, continuous culture with 10% FBS produces oncogenic stress in senescent MEFs, triggering tetraploidization. Thus, even though both are growth arrested (at least in total cell numbers) with senescent morphology at the same culture passage (P9) (Fig. S1), MEFs under tSD-3T3 conditions are continuously quiescent with genomic stability, while MEFs under Std-3T3 conditions develop tetraploidy (Fig. 1A, C), posing a question in DNA lesion status that induces chromosomal bridge formation and tetraploidization [10].

γH2AX foci accumulate in cells developing genomic instability but not in cells preserving diploidy

To determine the DNA lesion status induced by accelerated growth stimulation, γH2AX foci were compared in growth-arrested MEFs (P9) under both conditions (Fig. 1D). As expected, MEFs that developed tetraploidy under Std-3T3 conditions accumulated γH2AX foci, with some carrying over into the G2/M phases (Fig. 1E). This resulted in chromosome bridge formation (Fig. 1F) with the resulting tetraploidization that is initially observed with binucleated tetraploidy (Fig. 1F). On the other hand, quiescent MEFs that preserved genomic stability under tSD-3T3 conditions did not develop γH2AX foci (Fig. 1D), indicating that genomic stability is preserved under no γH2AX signal. However, it was still unclear why quiescent MEFs under tSD-3T3 conditions do not accumulate γH2AX foci because senescent cells are known to generally accumulate irreparable DNA lesions [13,14].

To address why γH2AX foci do not form under tSD-3T3 conditions, the expression level of H2AX at P9 was determined. As shown in Figure 1G, a remarkable reduction in H2AX expression was observed in quiescent MEFs at P9 while MEFs that developed tetraploidy under Std-3T3 conditions showed significantly higher H2AX expression than quiescent MEFs. This illustrates an association between H2AX levels and the cellular and genomic status, in that cells with largely diminished H2AX expression preserve stable diploidy and a quiescent status, while cells with residual H2AX expression and with γH2AX foci develop genomic instability and immortality (Fig. 1H). Importantly, H2AX-KO cells exhibited impaired DNA repair, growth retardation, and elevated genomic instability [24–28], phenotypes reminiscent of senescent cells. Therefore, it will be critical to determine how H2AX-status is regulated to produce quiescence and induce genomic instability.

H2AX is generally diminished in quiescent cells

To address whether H2AX diminution is a general occurrence, H2AX expression was compared in normal human fibroblasts (NHFs) and MEFs. Decreased H2AX was observed in both cell types at growth-arrested stage after serial proliferation (Fig. 2A, B), suggesting that this process is conserved between humans and mice. In addition, H2AX diminution was also observed in many organs of adult mice, including the liver, spleen, and pancreas (Fig. 2C, D; Fig. S2). Thus, H2AX is generally reduced in quiescent cell chromosomes both *in vitro* and *in vivo*.

H2AX is also diminished during premature senescence induced by DNA damage. Using early passage MEFs (P2), H2AX diminution was observed when senescence was induced by treatment with hydroxyurea (HU) to induce DNA replication stress (Fig. 2E) and with the radiomimetic DNA-damaging agent, neocarzinostatin (Fig. S3). This most likely occurs because DNA repair is coupled with H2AX release and chromatin remodeling [29–31]. Together with results showing a decrease in H2AX transcript levels in senescent MEFs (Fig. S4), these results indicate that decreased amounts of H2AX protein in senescing cells is ascribed to a decrease in H2AX transcript levels and DNA damage.

To directly address the impact of H2AX reduction, H2AX was knocked down in early passage NHFs, which induced cellular quiescence with senescent cell characteristics; cells adopted a flattened and enlarged morphology and showed an increase in senescence-associated β-galactosidase activity (Fig. 2F). Since the knockdown of H2AX in 293T cells induced growth arrest without inducing a senescent morphology (data not shown), it is likely that the effect of H2AX diminution is primarily due to quiescence induction and potentially a normal consequence of senescence in normal cells.

Immortalized cells develop following tetraploidization when H2AX status and growth activity are restored

The above results illustrate that cellular quiescence is produced when cells maintain stable diploidy and diminished H2AX

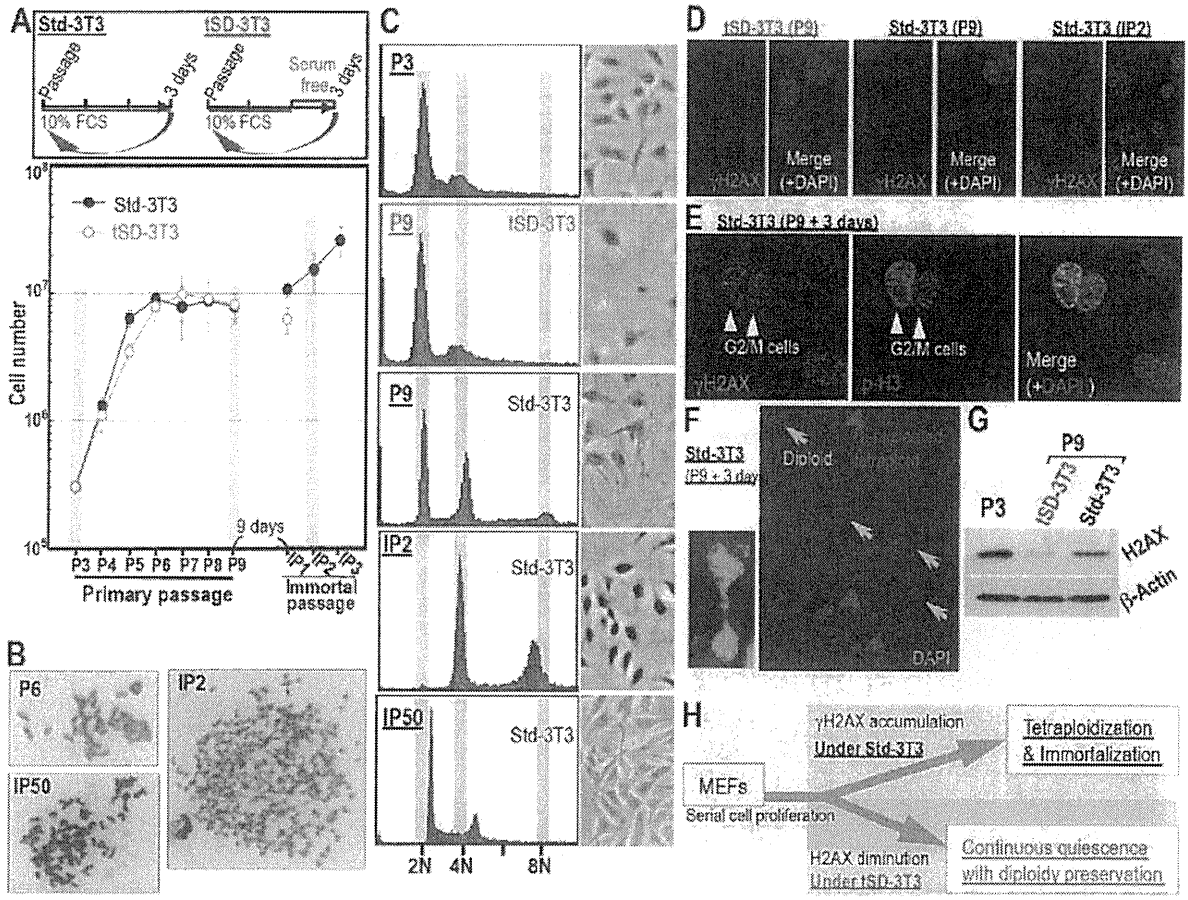

Figure 1. Immortality with tetraploidy is blocked in quiescent cells with diploidy, diminished H2AX, and no γH2AX foci. A. Growth curves of MEFs cultured under the standard 3T3 protocol (Std-3T3) or the T3 protocol with temporary serum deprivation (tSD-3T3) as schematically shown. MEFs under Std-3T3 conditions were immortalized, whereas MEFs cultured under tSD-3T3 conditions were not. **B** Genomic instability developed in immortalized MEFs (IP2) under Std-3T3 conditions. **C.** Genomic status was determined by flow-cytometry at the indicated conditions and passages. Representative images are shown. Tetraploidy development was blocked under tSD-3T3 conditions, while tetraploidy had already developed in growth-arrested MEFs at P9 under Std-3T3 conditions (see increasing 4N and 8N peaks). **D.** DNA lesions identified by γH2AX foci spontaneously accumulated in MEFs developing tetraploidy and immortality (P9) under Std-3T3 conditions as well as in immortal cells (IP2), while MEFs that maintained quiescent status with genomic stability under tSD-3T3 conditions contained no foci. **E.** DNA lesion-carryover into the G2-M phases was determined for lesions that spontaneously accumulated in senescent MEFs under Std-3T3 conditions. DNA lesions in senescing MEFs are also observed in the G2-M phases determined by phosphorylated H3. **F.** Chromosome bridge formation (Left panel) is observed in association with DNA lesion-carryover into the G2-M phases under Std-3T3 conditions with the resulting accumulation of bi-nucleated tetraploidy (Right panel: red arrow heads). Representative images are shown. **G.** The total H2AX level at P9 under each condition was determined. Whereas a significant reduction in H2AX expression was observed in MEFs with genomic stability under tSD-3T3 conditions, MEFs that developed immortality and genomic instability under Std-3T3 conditions did not show a significant decrease in H2AX expression. **H.** A model of the life-cycle of MEFs undergoing quiescence or developing immortality. While quiescent MEFs preserve diploidy and show diminished H2AX levels, MEFs developing immortality exhibited γH2AX foci accumulation.

doi:10.1371/journal.pone.0023432.g001

expression. In these cells, the H2AX level is less than 100-fold compared to that in actively growing cells. To study the effect of growth stimulation in cells with an H2AX-diminished quiescent status, complete medium (DMEM with 10% FBS) was added to quiescent MEFs prepared under tSD-3T3 conditions (Fig. 3A–C). In these cells, cell-cycle progression was initiated with the expression of PCNA and histones H3 and H2AX, which led to γH2AX foci formation (Fig. 3D, E). Abrogating quiescent status with complete medium resulted in the establishment of immortalized MEFs with tetraploidy (Fig. 3A–C). However, it took 30 days to initiate immortal passage in H2AX-diminished quiescent MEFs, while immortality was acquired in only 9 days for P9 MEFs under Std-3T3 conditions, suggesting that the H2AX-diminished quiescent status protected cells from immortalization. Supporting this argument, primary MEFs transfected with an H2AX expression vector also acquired immortality at an accelerated rate (Fig. S5A–C). Such H2AX-overexpression may induce the effect of DNA replication stress because immortality in H2AX-overexpressing MEFs were again developed with tetraploidy (Fig. S5D,E). Unexpectedly, H2AX status was totally recovered in actively growing, immortalized MEFs (Fig. 3F, G), which illustrates the association of H2AX status with growth activity.

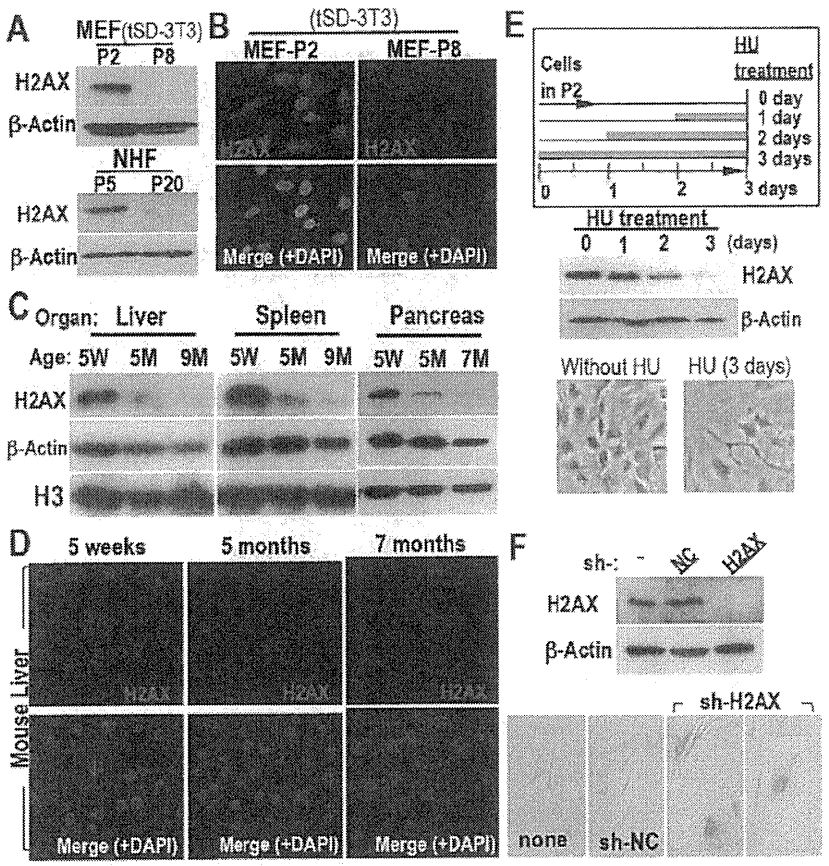

Figure 2. Quiescent cell-status is induced with H2AX diminution both *in vitro* and *in vivo*. **A,B** H2AX expression in growth-arrested cells (P8 for MEFs under tSD-3T3 conditions, P20 for NHFs) was determined by Western blotting (**A**) and immunofluorescent staining (**B**), revealing H2AX diminution in both types of growth-arrested cells. **C,D** H2AX diminution was also measured in adult mice organs by Western blotting (**C**) and in liver sections by immunofluorescent staining (**D**). Samples were prepared from five week (5W), five month (5M) and seven- or nine-month-old mice (7M or 9M). **E.** The involvement of H2AX diminution in DNA damage-induced premature senescence was determined after 0.2 mM HU treatment. Orange bars indicate the periods of HU treatment. Premature damage-induced senescence was observed with H2AX diminution, in which cells were flattened and enlarged, morphology typical of senescent cells. **F.** The effect of H2AX knockdown on senescence was determined in NHFs. Senescence was directly induced by H2AX knockdown in NHFs. H2AX status and senescence was determined by Western blotting (top) and SA-β-gal activation, and cells exhibited a flattened and enlarged morphology (bottoms), respectively.
doi:10.1371/journal.pone.0023432.g002

However, this also poses the question of how the down-regulation of H2AX expression in quiescent MEFs is reversed after immortalization.

Immortalized cells no longer achieve H2AX diminution-associated quiescent status

To explore the effects of the change in H2AX status, the response of H2AX to DNA replication stress was compared between primary and immortalized MEFs. While H2AX in primary MEFs was down-regulated after HU treatment, this did not occur in immortalized MEFs (Fig. 3H), which indicates that H2AX diminution-associated quiescent cell status is not inducible after immortalization. Thus, quiescent status is preserved in cells with diminished H2AX expression and stable diploidy but is abrogated under continuous growth stimulation, inducing cell cycle progression and γH2AX foci formation, and eventually leading to immortality with tetraploidy and H2AX recovery. Since the Arf/p53 module is specifically mutated during MEF immortalization [22], p53 might be involved in H2AX down-regulation. In fact, unlike senescent normal cells, H2AX expression is relatively high (2–20% of total H2A) in cancer cells as well as in growing NHFs (10%) [28].

H2AX diminution-associated quiescent status is produced by p53 and prohibits the development of immortality

To determine the involvement of p53 in H2AX down-regulation, *p53* knockout (KO) MEFs were cultured. Unlike normal primary MEFs, but similar to immortalized MEFs (Fig. 3H), H2AX expression in primary *p53*-KO-MEFs was not decreased by HU treatment (Fig. 4A). Furthermore, *p53*-KO-MEFs continuously grew, without change in H2AX status even under tSD-3T3 conditions (Fig. 4B, C). This indicates that H2AX in wild-type (WT)-MEFs is down-regulated by p53 to

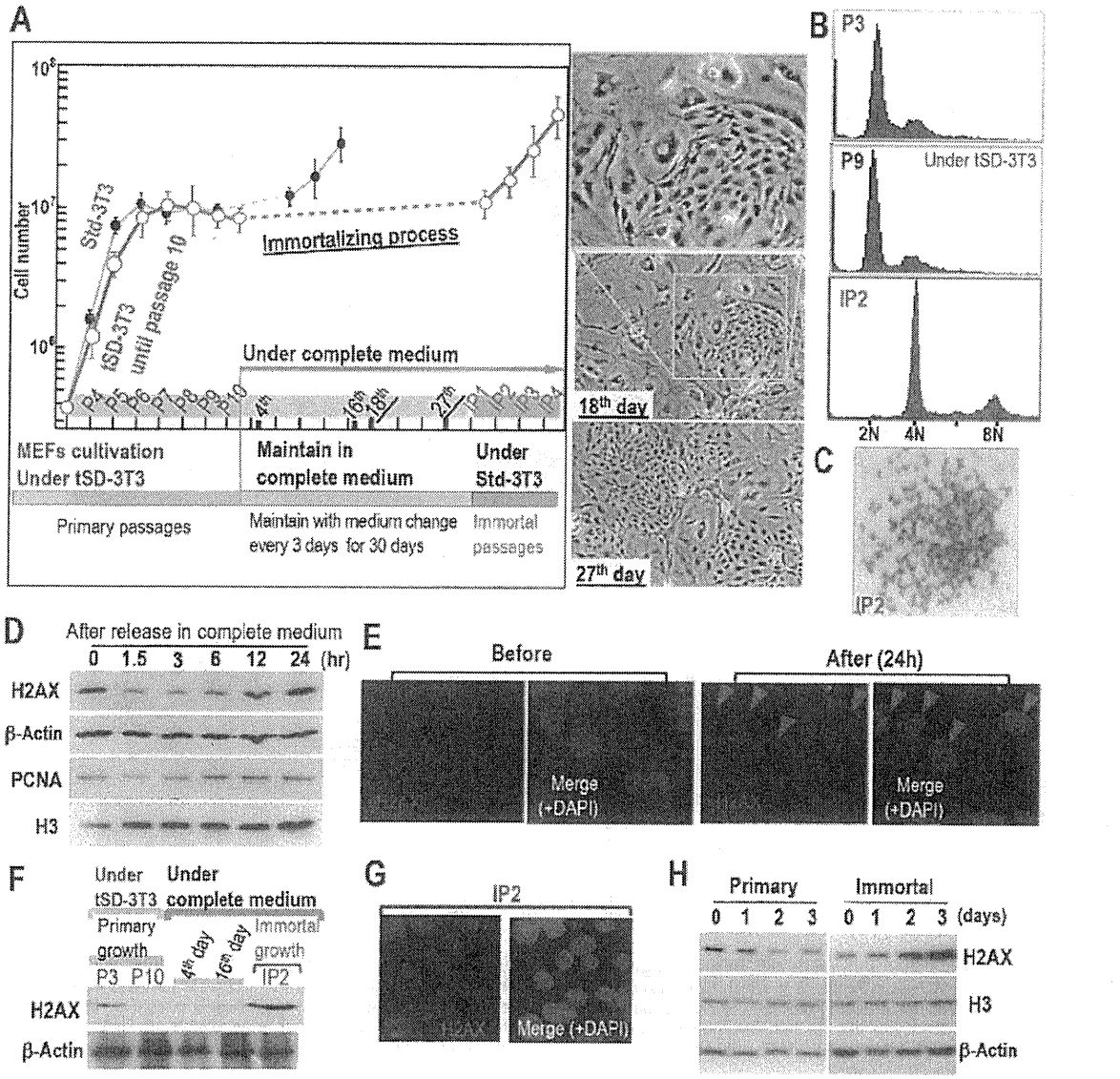

Figure 3. H2AX-diminished quiescent cell-status is abolished by continuous growth stimulation with accompanying H2AX recovery. A. Quiescent MEFs with diminished H2AX expression were cultured under tSD-3T3 conditions until P10. They were then exposed to complete medium, which was changed every three days for 30 days. Immortal passages were started under Std-3T3 conditions (red circles). MEFs cultured under the Std-3T3 conditions (black circles) as in Figure 1a were superimposed for comparison of the time needed to acquire immortality. Representative images of MEFs during the process of acquiring immortality are also shown. **B,C.** Tetraploidy development in immortalized MEFs (IP2) was observed by flow-cytometry (**B**) and Giemsa staining (**C**). **D.** Growth acceleration-associated cell cycle progression and H2AX induction. To determine the effect of serum induction on H2AX expression and cell cycle progression, senescent MEFs at P8 were incubated in serum-free medium for 24 h and harvested after exposure to complete medium for various times. H2AX expression increased with increasing PCNA and histone H3, which suggests that the expression of these chromatin factors was associated with S phase entry. To detect H2AX levels in these MEFs at P8, the H2AX signal was visualized by longer exposure. **E.** DNA lesions characterized by γH2AX foci were induced in MEFs (red arrowheads) after exposure to complete medium as in **D**. **F,G.** H2AX status in immortalized MEFs was determined by Western blotting (**F**) and immunofluorescence (**G**), revealing H2AX recovery. **H.** DNA replication stress-associated H2AX diminution was compared between normal and immortalized MEFs as in Figure 2E, in which H2AX was not down-regulated after immortalization.
doi:10.1371/journal.pone.0023432.g003

induce cellular quiescence and is recovered in immortalized MEFs in association with tetraploidization and mutation of the Arf/p53 module. Although *p53*-KO-MEFs did not undergo H2AX diminution-mediated growth arrest, these MEFs still exhibited a senescent morphology (Fig. 4D, see P8) and subsequently achieved an immortalized morphology (P14), which suggests the immortalization of *p53*-KO-MEFs via the senescent stage without growth arrest. This also indicates that a quiescent cell status is induced by p53 to protect cells from immortality.

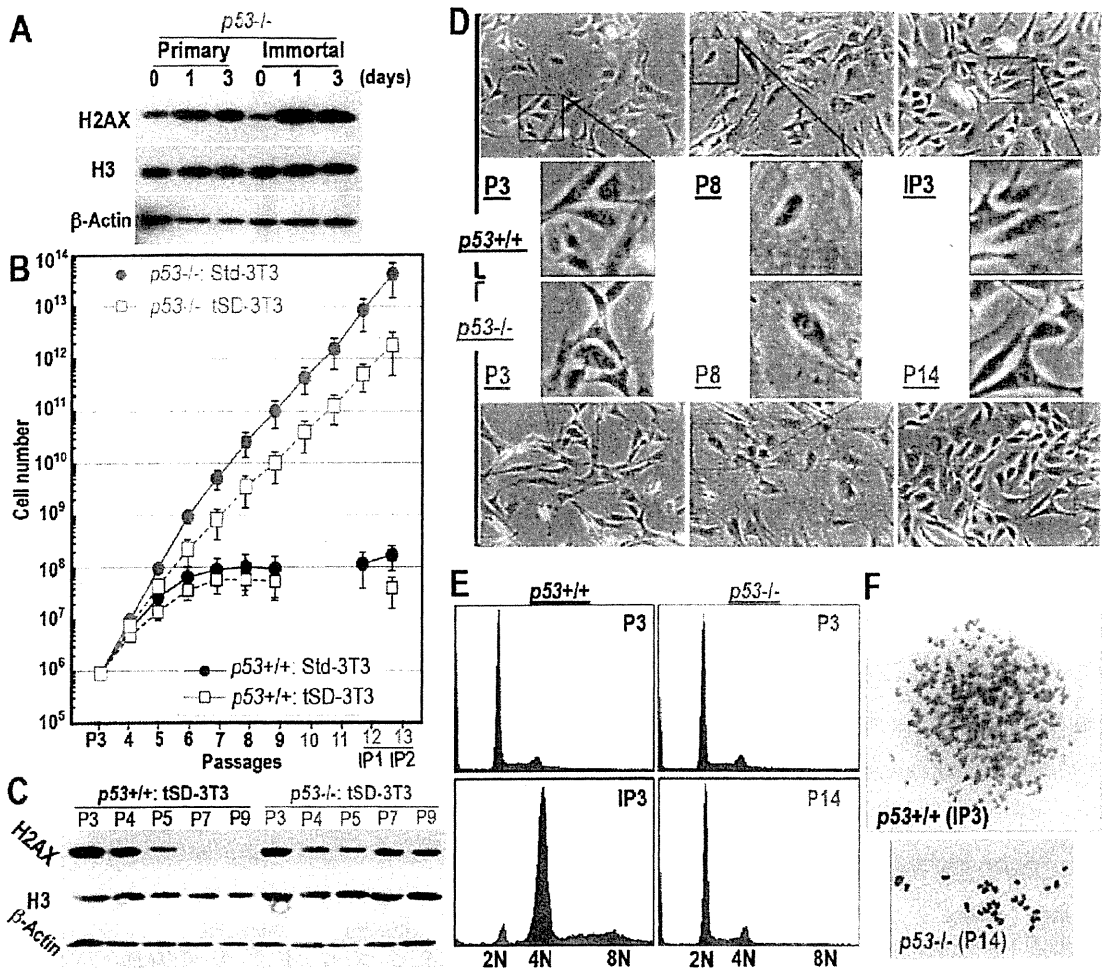

Figure 4. H2AX-diminished quiescent cell status is regulated by p53. A. DNA replication stress-associated H2AX diminution status was determined in *p53*-KO MEFs as in Figure 2E, in which H2AX was not down-regulated, even in primary MEFs. **B–F.** Primary *p53*-KO MEFs were cultured during the senescing and immortalizing processes (**B**). H2AX status was determined by Western blotting (**C**), morphological assessment (**D**), genomic status determined by flow-cytometry (**E**), and chromosome spread (**F**). Although *p53*-KO MEFs never showed major changes in H2AX expression, tetraploidization or growth arrest, *p53*-KO MEFs still exhibited a senescent morphology (P8) before achieving an immortalized morphology (P14).
doi:10.1371/journal.pone.0023432.g004

Mutation of the Arf/p53 module is induced with tetraploidization, triggered by DNA replication stress under moderately decreased H2AX levels in normal cells

Whereas *p53*-KO-MEFs are immortalized with diploidy (Fig. 4E, F), WT-MEFs are never immortalized only after tetraploidization [10] (Fig. 1B, C; Fig. 3B, C; Fig. 4E, F) and loss of Arf/p53 [22]. This suggests that the mutation of the Arf/p53 module in WT-MEFs is induced during tetraploidization. Supporting this argument, p53-dependent quiescence produced by diminished H2AX is maintained under diploidy preservation but abrogated after tetraploidization with mutation in the Arf/p53 module and the resulting H2AX recovery (Fig. 3). Therefore, normal WT-MEFs are protected from immortalization by a quiescent cell status, as long as the genome is preserved in diploidy. However, under continuous growth stimulation, tetraploidization also spontaneously arises in WT-MEFs but, unexpectedly, not in *p53*-KO-MEFs.

As tetraploidization was observed at the senescent stage under conditions of continuous growth stimulation that induce DNA replication stress (Fig. 3), the underlying reason for tetraploidization in WT-MEFs but not in *p53*-KO-MEFs might be associated with the repair deficiency that also occurs in an H2AX-diminished background. To examine the tetraploidization risk under an H2AX-diminished background, MEFs of each type were treated with HU for 36 hours and the incidence of bi-nucleated tetraploidy formation was compared (Fig. 5A). As expected, HU treatment-associated H2AX diminution (Fig. 2E) resulted in tetraploidization in primary WT-MEFs but not in immortalized WT-MEFs or p53-KO-MEFs (Fig. 5A). Thus, although normal cells become quiescent with largely diminished H2AX under diploidy, senescing cells with residual H2AX under growth stimulating conditions are potentially at risk of developing tetraploidy in response to DNA replication stress.

Finally, to address changes in DNA replication stress-sensitivity during serial proliferation of normal MEFs, the repair efficiencies

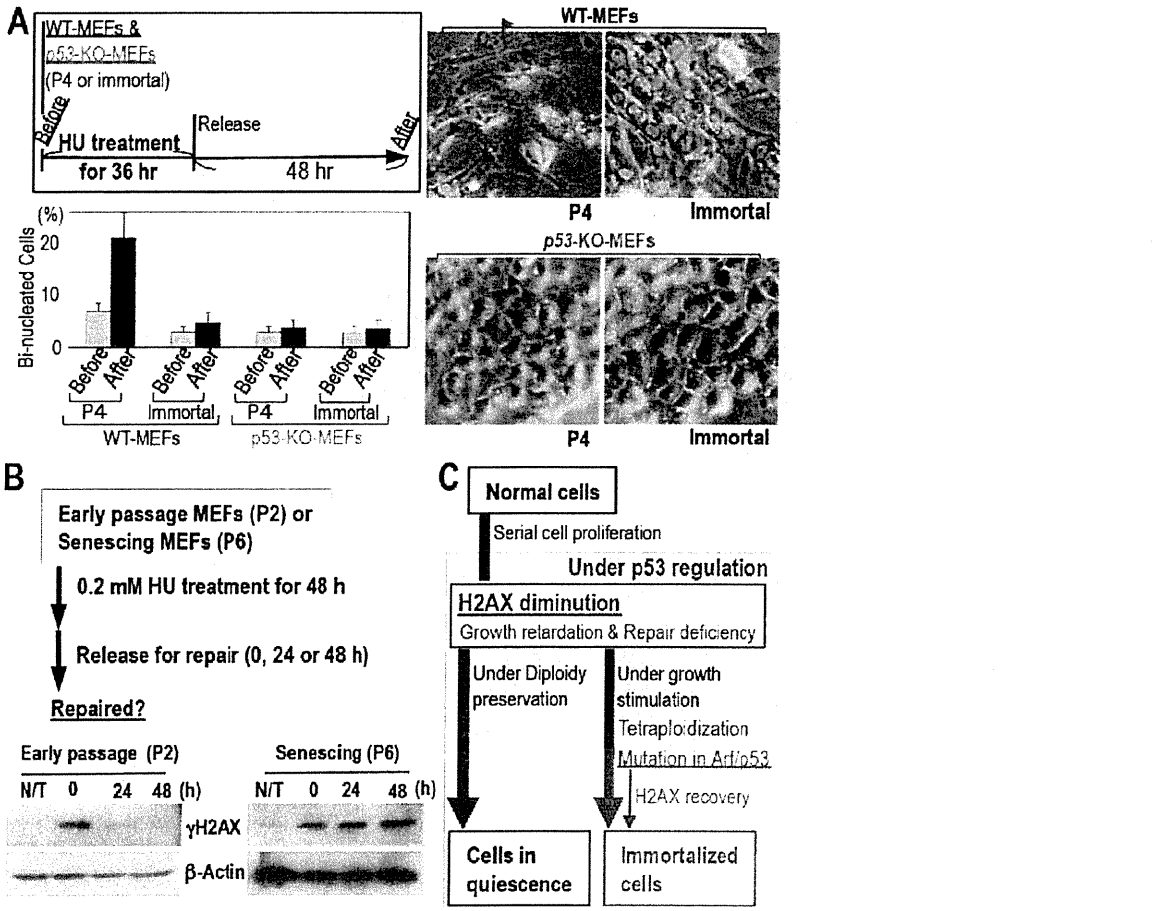

Figure 5. Increased risk of tetraploidization in normal MEFs. A. DNA replication stress-associated tetraploidization was determined in MEFs (P4) with the formation of bi-nucleated tetraploidy (red arrowhead) after 0.2 mM HU treatment as illustrated (top-left panel). Tetraploidization was efficiently induced during primary growth but not in immortalized MEFs or *p53*-KO-MEFs. **B.** Repair efficiencies of DNA replication stress-associated lesions were compared between early passage (P2) and senescing MEFs (P6) after 48 h hydroxyurea (HU) treatment. γH2AX signal was used as a marker of DNA lesions, in which γH2AX signal and β-Actin signals in senescing MEFs (P6) were detected only with over-exposure compared to early passage MEFs (P2), due to decreased H2AX levels during senescence. The reduction in γH2AX signal after release was only evident in early passage MEFs, which suggests that senescing cells are defective in resolving DNA replication stress. **C.** A model of MEFs under serial cell proliferation either undergoing quiescence or developing immortality. While MEFs that maintain quiescence and diploidy show diminished H2AX levels, MEFs developing immortality accumulate γH2AX foci.
doi:10.1371/journal.pone.0023432.g005

of DNA replication stress-associated lesions were compared between early passage and senescent MEFs with the decay of the γH2AX signal after release from HU treatment (Fig. 5B). Unlike early passage MEFs (P2), senescing MEFs (P6) were deficient in repairing HU-associated DNA lesions (Fig. 5B), in which MEFs show slow cell-cycle progression and residual H2AX expression. This is in contrast to quiescent MEFs with largely diminished H2AX level that show neither detectable cell cycle progression nor DNA replication stress. Thus, normal cells under serial proliferation decrease H2AX expression; thereby, cells slow growth activity and become defective in DNA repair. In such cells, cellular homeostasis is preserved by quiescence under largely diminished H2AX level regulated by p53 as long as diploidy is preserved. However, these cells are simultaneously at increased risk of tetraploidization with p53 dysfunction under continuous growth acceleration, resulting in the development of immortality and recovery of H2AX activity and cell growth (Fig. 5C).

Discussion

The results of this study revealed the following novel concepts: (i) normal cells generally achieve quiescent status with diminished H2AX level both *in vitro* and *in vivo*, and this is regulated by p53; (ii) growth arrested normal cells with senescent morphology can be defined as either (a) those in a continuous quiescent status with largely diminished H2AX level or (b) those in a transient status with inducing genomic instability and the resulting onset of immortality, under which cells accumulate γH2AX foci; (iii) to protect cells from immortality, one of the critical roles of p53 is the induction of growth-arrest via the down-regulation of H2AX with cellular quiescence. Cells in H2AX diminution-associated quiescence are shown in the cause of mature and premature senescence, during which cells show senescent morphology (Fig. S1), probably because these cells are repair defective (Fig. 5B). However such repair deficiency is also associated with genomic instability

development under accelerated growth stimulation, resulting in immortality acquisition with Arf/p53 module mutation and H2AX recovery.

Since growth-arrested cellular status with senescent morphology is directly induced by H2AX-knockdown (Fig. 2F), H2AX down-regulation is involved in a cause of quiescent cellular status. On the other hand, residual H2AX-expression in senescent cells is an associated effect for tetraploidization and immortalization: residual H2AX in senescent cells are only observed under accelerated growth stimulation (Figs. 1 and 3), under which cells are subjected to DNA replication stress and exhibit γH2AX, resulting in tetraploidization. Thus, even though cells are morphologically senescent with no growth in total cell number, cellular statuses could be either cells developing genomic instability under continuous growth acceleration (Std-3T3) or continuously quiescent cells under occasional arrest (tSD-3T3).

Unlike highly accumulated p53 that induces apoptosis, the Arf/p53 module under normal conditions functions for longevity by suppressing tumors in mice and giving protection from immortalization in MEFs [22]. Here, our results illustrated that such cellular status is produced with H2AX diminution-associated quiescence by protecting from immortalization under normal p53 regulation but is abrogated by Arf/p53 module mutation that is induced with tetraploidization under continuous growth stimulation, resulting in recovery of H2AX and growth activity. Unlike cells undergoing apoptosis, cells preserving quiescence under normal conditions do not accumulate p53 protein [10], which is probably associated with p53 function expression for quiescent status preservation but not for apoptosis induction. Intriguingly, such p53-dependent H2AX diminution was only observed after cells reach growth arrest both *in vivo* and *in vitro* but not growing cells in early passages and in organs from young mice (Fig. 2). In accordance with this, the expression of p53 targets Sidt2 and Phlda3, which are likely associated with tumor suppression [32], were elevated after cells become H2AX diminution-associated quiescent (P7) compared to cells in early passage (P3) (Fig. S6). However, similar to p53 protein, the increase in p53 transcript is also limited (Fig. S6). Thus, p53 function is expressed for apoptosis with accumulated p53, otherwise for H2AX-diminution associated quiescent status preservation under normal regulation without accumulating p53.

Except for tumors associated with specific chromosomal translocation, development of most cancers as well as *in vitro* cellular transformation is associated with genomic instability of either CIN or MIN [2,3]. Importantly, tetraploidization, a major initial form of CIN under a mismatch repair proficient background is induced with oncogenic stress by accelerated S-phase entry [10], leading to immortality acquisition in MEFs with mutation in the Arf/p53 module. Here, our results showed that quiescence could be preserved with largely diminished H2AX and diploidy preservation under the regulation of p53. Although H2AX down-regulation is only observed under functional p53 regulation, it is still unclear how p53 down-regulates H2AX. Our results showed the reduction of total H2AX transcript during the senescing process (Fig. S4) and a damage-induced decrease of H2AX protein under functional p53 regulation (Fig. 2E; Fig. 4A, B). Although p53 role for H2AX down-regulation is unclear, the regulation might be indirect because (1) there is no p53-binding site on the *H2AX* promoter, (2) there is no signal of the *H2AX* gene with ChIP-on-CHIP analyses against p53 [33], (3) H2AX expression does not associate with the activation level of p53 as we observed no association between H2AX expression and p53 activation (Fig. S7).

Together, our results provide a rationale for the regulation of cellular homeostasis preservation. By prohibiting immortality development and preserving quiescent cell status, p53 induces an H2AX diminution-mediated quiescent status. However, this status is abrogated by continuous growth stimulation, which results in the induction of genomic instability with mutation of the Arf/p53 module, which leads into H2AX recovery, the restoration of growth activity, and immortality acquisition (Fig. 5C).

Methods

Ethics Statement

Mice were treated in accordance with the Japanese Laws and the Guidelines for Animal Experimentation of National Cancer Center. All experiments were approved by The Committee for Ethics in Animal Experimentation of National Cancer Center (approval ID numbers: A59-09 and T07-038).

Cell culture and tissue samples

Cells were cultured as described previously [34]. Both wild-type and *p53*-KO MEFs were prepared from day 13.5 embryos of wild type and $p53^{(+/-)}$ mice [35] as previously described [34] and cultured under the standard 3T3 (Std-3T3) passage protocol [36] or with the following modifications: tSD-3T3. Senescing MEFs (P6 or P8) were maintained under tSD-3T3 conditions for the experiments shown in Figures 2, 3, 4, 5. NHFs (normal human umbilical cord fibroblasts; HUC-F2, RIKEN BRL Cell Bank) were cultured under Std-3T3 conditions. Resveratrol treatment of NHFs was performed as for MEFs. For the H2AX shRNA study, the reported sequence oligonucleotide [37,38] was inserted into the pSuper.retro.puro vector (Oligoengine) and the shRNA virus was then prepared using 293T cells. The virus was infected into NHF cells and selected with puromycin. Mouse tissue samples were prepared from mice at the ages indicated (Sankyo Labo Service).

DNA damage and induction of replication stress

DSB damage was induced by neocarzinostatin (Pola Pharma, Tokyo, Japan) treatment. For induction of DNA replication stress, MEFs were treated with hydroxyurea (HU).

Antibodies, immunostaining and Western blotting

Antibodies against γH2AX (JBW301, Upstate Biotechnology) and H2AX (Bethyl) were used for immunostaining and Western blot analysis. Antibodies against β-actin (AC-74, Sigma), PCNA (Santa Cruz) and histone H3 (ab1791, Abcam) were used for Western blot analysis. Prior to immunostaining with primary and secondary antibodies, cells were fixed with 4% paraformaldehyde for 10 min and permeabilized with 0.1% Triton X-100/PBS for 10 min. Western blot analysis and confocal microscopy were performed as described previously [10].

Transcription level analyses with RT-PCR

Total RNA was extracted from MEFs with the RNeasy system (Sigma). RNA (0.8 μg) was reverse-transcribed using a cDNA Archive kit (Applied Biosystems) and subjected to PCR. The following PCR primers were used: H2axf, 5′-TTGCTTC-AGCTTGGTGCTTAG-3′; H2axr, AACTGGTATGAGGC-CAGCAAC; β-actinf, CATCCAGGCTGTGCTGTCCCTGTA-TGC; and β-actinr, GATCTTCATGGTGCTAGGAGCCA-GAGC; Trp53-F, CGGATAGTATTTCACCCTCAAGATC-CG; Trp53-R, AGCCCTGCTGTCTCCAGACTC; Sidt2-F, CGGAAGGCTGGTTTCTGAGTTTCCG; Sidt2-R, CTGTA-AACGCCAAGGACCAGAA; Phlda3-F, CGGTCCATCTAC-

TTCACGCTAGTGACGG; Phlda3-R, TGGATGGCCTGTTGATTCTTGA; Gapdh-F, AACTTTGGCATTGTGGAAGG; Gapdh-R, ATGCAGGGATGATGTTCTGG. The amplified products by AmpliTaq Gold (Applied Biosystems) were separated on a 2% agarose gel and visualized with ethidium bromide. Otherwise, real-time PCR assay was carried out using Power SYBER green PCR Master kit (ABI).

Chromosome spreads

Mitotic cells were prepared by treatment with 20 ng/ml nocodazole for 6 h and then collected. The collected cells were swollen hypotonically with 75 mM KCl for 15 min, and then fixed with Carnoy's solution (75% methanol/25% acetic acid) for 20 min. After changing the fixative once, the cells were dropped in Carnoy's solution onto glass slides and air-dried. The slides were stained with 4% Giemsa (Merck) solution for 10 min, washed briefly in tap water, and air-dried.

Supporting Information

Figure S1 Representative images of MEFs during the lifespan. MEFs cultivated as in Figure 1A top lead into either immortality development under Std-3T3 or quiescence preservation under tSD-3T3. After serial cultivation, MEFs become morphologically senescent, i.e., flattened and enlarged morphology (P9) under both Std-3T3 and tSD-3T3 conditions. While continuous MEF-culture under tSD-3T3 preserved the quiescent status with continuously senescent morphology, continuous MEF-culture under Std-3T3 lead to the sporadic emergence of immortalized colony from the senescent MEFs. Immortalized MEFs (IP2) are morphologically escaped from senescence and rather similar to that in early passage (P3).
(TIF)

Figure S2 H2AX diminution is also observed in adult mice organs. Samples were prepared from five week (5W), five month (5M) and seven- or nine-month-old mice (7M or 9M). Compared to five months old organs, H2AX protein level is diminished in Testis (9M), Brain (7M), and Colon (7M), in which the diminution levels are lower than those in Liver, Spleen, and Pancreas. In Heart and Thymus, H2AX levels did not altered the alteration in through 5 weeks old to 7 or 9 months old.
(TIF)

Figure S3 H2AX diminution is also shown in damage induced premature senescence. Premature senescence was induced with NCS treatment as shown schematically in the top, in which each red arrowhead represents 100 ng/μl NCS treatment. Premature senescence by damage was induced with H2AX diminution, in which cells showed typical senescent morphology of flattened and enlarged.
(TIF)

Figure S4 H2AX transcript is decreased in quiescent MEFs. Decrease in H2AX mRNA level in senescing MEFs was observed by RT-PCR (right panel) and is compared with protein diminution (left panel).
(TIF)

Figure S5 H2AX over-expression accelerates immortality development in MEFs with tetraploidy. A. Experimental scheme of H2AX over expression. After transfection of H2AX-over expressing (H2AX-OE) or empty control vectors into early passage MEFs (P3), the transformed MEFs were selected, re-plated, and maintained in complete medium until immortalized cells appeared. **B.** Growth curves of MEFs during the experiments in A. MEFs before transfection and re-plating, MEFs transfected with H2AX-over-expressing vector, and MEFs transfected with empty control vector are indicated by black closed squares, red open circles, and black open diamonds, respectively. MEFs over-expressing H2AX showed accelerated development of immortality. **C.** H2AX status was determined as indicated in the figure. Although senescence was induced in the transfected and selected MEFs, H2AX over-expressing MEFs show higher levels of H2AX after the selection resulting in the development of immortality with H2AX recovery. **D.** Representative MEF images during accelerated immortality development with H2AX over-expression and controls. MEFs transfected with the H2AX over-expressing vector showed an efficient escape from senescence, while MEFs carrying the negative control vectors remained senescent with a flattened and enlarged morphology. **E,F.** Genomic instability status in immortalized MEFs (IP3) that were developed with H2AX over-expression was assessed by flow-cytometry (**E**) and Giemsa staining of M-phase chromosome (**F**).
(TIF)

Figure S6 p53 expression in senescing MEFs. To determine p53 expression in the cause of senescence, the expression levels of p53 and the targets (Sidt2 and Phlda3) that are likely associated with tumor suppression were compared between early passage (P2) and senescent MEFs (P7) under tSD-3T3 conditions. Along with H2AX diminution under p53 proficient background after serial cultivation, the expressions of Sidt2 and Phlda3 were observed in senescent MEFs (P7), in which the change in the expressed p53 transcript is limited.
(TIF)

Figure S7 p53 activation shown by miR34a expression in primary wt-MEFs after damage is not directly associated with H2AX expression levels at least for transcript regulation. A. To confirm p53 dependent DNA damage response, wt- and $p53^{-/-}$-MEFs in primary and immortal were treated with 200 ng/ml neocarzinostatin (NCS) for 6 hours and the expression of p53-target miR34a was assessed. As expected, miR34a expression was shown after NCS treatment in primary wt-MEFs (wild type) but neither in immortalized wt-MEFs nor in $p53^{-/-}$-MEFs. **B.** To determine the p53-activation associated change in the expression levels of H2AX transcript, mRNA levels of H2AX in MEFs treated as in **A** were analyzed. Whereas p53 is activated after NCS treatment in primary wt-MEFs, H2AX transcript levels were stable, suggesting no direct regulation by p53 transcription factor for H2AX expression. The PCR primers for miR34a were used from miRNA-specific primers (ABI) with snoRNA202 (ABI) for the control. Real-time PCR assay was carried out TaqMan microRNA assay kit (ABI).
(TIF)

Acknowledgments

We thank RIKEN BRL Cell Bank for the normal human umbilical cord fibroblast (NHF) cells (HUC-F2). We also thank K. Shimizu-Saito, M. Yanokura, and I. Kobayashi for technical support. We are grateful to S. Takeda, W. Bonner, P. Hsieh, K. Okamoto, and S. Nakada for critical reading of the manuscript and to T. Tsuzuki and Y. Nakatsu for critical discussion of the study.

Author Contributions

Conceived and designed the experiments: KY. Performed the experiments: YA H. Fuji H. Fukuda AI KS YY MS YI JU KY. Analyzed the data: H. Fuji KY. Contributed reagents/materials/analysis tools: SM NT YH HN MM. Wrote the paper: KY H. Fukuda HT.

References

1. Negrini S, Gorgoulis VG, Halazonetis TD (2010) Genomic instability–an evolving hallmark of cancer. Nat Rev Mol Cell Biol 11: 220–228.
2. Lengauer C, Kinzler KW, Vogelstein B (1997) Genetic instabilities in colorectal cancers. Nature 386: 632–627.
3. Lengauer C, Kinzler KW, Vogelstein B (1998) Genetic instabilities in human cancers. Nature 396: 643–649.
4. Stephans PJ, Greenman CD, Fu B, Yang F, Bignell GR, et al. (2011) Massive genomic rearrangement acquired in a single catastrophic event during cancer development. Cell 144: 27–40.
5. Vitale I, Galluzzi L, Senovilla L, Criollo A, Jemaà M, et al. Illicit survival of cancer cells during polyploidization and depolyploidization. Cell death differ, doi: 10.1038/cdd.2010.145.
6. Danes BS (1978) Increased in vitro tetraploidy: tissue specific within the heritable colorectal cancer syndromes with polyposis coli. Cancer 41: 2330–2334.
7. Dutrillaux B, Gerbault-Seureau M, Remvikos Y, Zafrani B, Prieur M (1991) Breast cancer genetic evolution: I. Data from cytogenetics and DNA content. Breast Cancer Res Treat 19: 245–255.
8. Heselmeyer K, Schröck E, du Manoir S, Blegen H, Shah K, et al. (1996) Gain of chromosome 3q defines the transition from severe dysplasia to invasive carcinoma of the uterine cervix. Proc Natl Acad Sci USA 93: 479–484.
9. Maley CC, Galipeau PC, Li X, Sanchez CA, Paulson TG, et al. (2004) The combination of genetic instability and clonal expansion predicts progression to esophageal adenocarcinoma. Cancer Res 64: 7629–7633.
10. Ichijima Y, Yoshioka K, Yoshioka Y, Shinohe K, Fujimori H, et al. (2010) DNA lesions induced by replication stress trigger mitotic aberration and tetraploidy development. PLoS One 5: e8821.
11. Bartkova J, Horejsí Z, Koed K, Krämer A, Tort F, et al. (2005) DNA damage response as a candidate anti-cancer barrier in early human tumorigenesis. Nature 434: 864–870.
12. Gorgoulis VG, Vassiliou LV, Karakaidos P, Zacharatos P, Kotsinas A, et al. (2005) Activation of the DNA damage checkpoint and genomic instability in human precancerous lesions. Nature 434: 907–913.
13. Sedelnikova OA, Horikawa I, Zimonjic DB, Popescu NC, Bonner WM, et al. (2004) Senescing human cells and ageing mice accumulate DNA lesions with unrepairable double-strand breaks. Nature Cell Biol 6: 168–170.
14. Nakamura AJ, Chiang YJ, Hathcock KS, Horikawa I, Sedelnikova OA, et al. (2008) Both telomeric and non-telomeric DNA damage are determinants of mammalian cellular senescence. Epigenetics Chromatin 1: 6.
15. Geigl JB, Langer S, Barwisch S, Pfleghaar K, Lederer G, et al. (2004) Analysis of gene expression patterns and chromosomal changes associated with aging. Cancer Res 64: 8550–8557.
16. Sherr CJ, Weber JD (2000) The ARF/p53 pathway. Curr Opin Genet Dev 10: 94–99.
17. Sherr CJ (1998) Tumor surveillance via the ARF-p53 pathway. Genes Dev 12: 2984–2991.
18. Matheu A, Maraver A, Serrano M (2008) The Arf/p53 pathway in cancer and aging. Cancer Res 68: 6031–6034.
19. Tyner SD, Venkatachalam S, Choi J, Jones S, Ghebranious N, et al. (2002) p53 mutant mice that display early ageing-associated phenotypes. Nature 415: 45–53.
20. Maier B, Gluba W, Bernier B, Turner T, Mohammad K, et al. (2004) Modulation of mammalian life span by the short isoform of p53. Genes Dev 18: 306–319.
21. Varela I, Cadiñanos J, Pendás AM, Gutiérrez-Fernández A, Folgueras AR, et al. (2005) Accelerated ageing in mic deficient in Zmpste24 protease is linked to p53 signalling activation. Nature 437: 564–568.
22. Matheu A, Maraver A, Klatt P, Flores I, Garcia-Cao I, et al. (2007) Delayed ageing through damage protection by the Arf/p53 pathway. Nature 448: 375–379.
23. Parrinello S, Samper E, Krtolica A, Goldstein J, Melov S, et al. (2003) Oxygen sensitivity severely limits the replicative lifespan of murine fibroblasts. Nature Cell Biol 5: 741–746.
24. Bassing CH, Chua KF, Sekiguchi J, Suh H, Whitlow SR, et al. (2002) Increased ionizing radiation sensitivity and genomic instability in the absence of histone H2AX. Proc Natl Acad Sci USA 99: 8173–8178.
25. Celeste A, Petersen S, Romanienko PJ, Fernandez-Capetillo O, Chen HT, et al. (2002) Genomic instability in mice lacking histone H2AX. Science 296: 922–927.
26. Bronson R, Lee C, Alt WF (2003) Histone H2AX: A dosage-dependent suppressor of oncogenic translocations and tumors. Cell 114: 359–370.
27. Bassing CH, Alt FW (2004) H2AX May Function as an Anchor to Hold Broken Chromosomal DNA Ends in Close Proximity. Cell Cycle 3: 149–153.
28. Bonner WM, Redon CE, Dickey JS, Nakamura AJ, Sedelnikova OA, et al. (2008) GammaH2AX and cancer. Nature Rev Cancer 8: 957–967.
29. Tsukuda T, Fleming AB, Nickoloff JA, Osley MA (2005) Chromatin remodelling at a DNA double-strand break site in Saccharomyces cerevisiae. Nature 438: 379–383.
30. Keogh MC, Mennella TA, Sawa C, Berthelet S, Krogan NJ, et al. (2006) The Saccharomyces cerevisiae histone H2A variant Htz1 is acetylated by NuA4. Genes Dev 20: 660–665.
31. Ikura T, Tashiro S, Kakino A, Shima H, Jacob N, et al. (2007) DNA damage-dependent acetylation and ubiquitination of H2AX enhances chromatin dynamics. Mol Cell Biol 27: 7028–7040.
32. Brady CA, Jiang D, Mello SS, Johnson TM, Jarvis LA, et al. (2011) Distinct p53 transcriptional programs dictate acute DNA-damage responses and tumor suppression. Cell 145: 571–583.
33. Ceribelli M, Alcalay M, Viganò MA, Mantovani R (2006) Repression of new p53 targets revealed by ChIP on chip experiments. Cell Cycle 5: 1102–1110.
34. Yoshioka K, Yoshioka Y, Hsieh P (2006) ATR kinase activation mediated by MutSα and MutLα in response to cytotoxic O6-methylguanine adducts. Mol Cell 22: 501–510.
35. Tatemichi M, Tazawa H, Masuda M, Saleem M, Wada S, et al. (2004) Suppression of thymic lymphomas and increased nonthymic lymphomagenesis in Trp53-deficient mice lacking inducible nitric oxide synthase gene. Int J Cancer 111: 819–828.
36. Todaro GJ, Green H (1963) Quantitative studies of the growth of mouse embryo cells in culture and their development into established lines. J Cell Biol 17: 299–313.
37. Lukas C, Melander F, Stucki M, Falck J, Bekker-Jensen S, et al. (2004) Mdc1 couples DNA double-strand break recognition by Nbs1 with its H2AX-dependent chromatin retention. EMBO J 23: 2674–2683.
38. Dimitrova N, de Lange T (2006) MDC1 accelerates nonhomologous end-joining of dysfunctional telomeres. Genes Dev 20: 3238–3243.

JVI
Journals.ASM.org

Production of Infectious Chimeric Hepatitis C Virus Genotype 2b Harboring Minimal Regions of JFH-1

Asako Murayama,[a] Takanobu Kato,[a] Daisuke Akazawa,[a] Nao Sugiyama,[a] Tomoko Date,[a] Takahiro Masaki,[a] Shingo Nakamoto,[b] Yasuhito Tanaka,[c] Masashi Mizokami,[d] Osamu Yokosuka,[b] Akio Nomoto,[e]* and Takaji Wakita[a]

Department of Virology II, National Institute of Infectious Diseases, Shinjuku-ku, Tokyo, Japan[a]; Department of Medicine and Clinical Oncology, Graduate School of Medicine, Chiba University, Chuo, Chiba, Japan[b]; Department of Virology and Liver Unit, Nagoya City University Graduate School of Medical Sciences, Kawasumi, Mizuho, Nagoya, Japan[c]; The Research Center for Hepatitis and Immunology, National Center for Global Health and Medicine, Ichikawa, Chiba, Japan[d]; and Department of Microbiology, Graduate School of Medicine, University of Tokyo, Bunkyo-ku, Tokyo, Japan[e]

To establish a cell culture system for chimeric hepatitis C virus (HCV) genotype 2b, we prepared a chimeric construct harboring the 5′ untranslated region (UTR) to the E2 region of the MA strain (genotype 2b) and the region of p7 to the 3′ UTR of the JFH-1 strain (genotype 2a). This chimeric RNA (MA/JFH-1.1) replicated and produced infectious virus in Huh7.5.1 cells. Replacement of the 5′ UTR of this chimera with that from JFH-1 (MA/JFH-1.2) enhanced virus production, but infectivity remained low. In a long-term follow-up study, we identified a cell culture-adaptive mutation in the core region (R167G) and found that it enhanced virus assembly. We previously reported that the NS3 helicase (N3H) and the region of NS5B to 3′ X (N5BX) of JFH-1 enabled replication of the J6CF strain (genotype 2a), which could not replicate in cells. To reduce JFH-1 content in MA/JFH-1.2, we produced a chimeric viral genome for MA harboring the N3H and N5BX regions of JFH-1, combined with a JFH-1 5′ UTR replacement and the R167G mutation (MA/N3H+N5BX-JFH1/R167G). This chimeric RNA replicated efficiently, but virus production was low. After the introduction of four additional cell culture-adaptive mutations, MA/N3H+N5BX-JFH1/5am produced infectious virus efficiently. Using this chimeric virus harboring minimal regions of JFH-1, we analyzed interferon sensitivity and found that this chimeric virus was more sensitive to interferon than JFH-1 and another chimeric virus containing more regions from JFH-1 (MA/JFH-1.2/R167G). In conclusion, we established an HCV genotype 2b cell culture system using a chimeric genome harboring minimal regions of JFH-1. This cell culture system may be useful for characterizing genotype 2b viruses and developing antiviral strategies.

Hepatitis C virus (HCV) is a major cause of chronic liver disease (5, 13), but the lack of a robust cell culture system to produce virus particles has hampered the progress of HCV research (2). Although the development of a subgenomic replicon system has enabled research into HCV RNA replication (15), infectious virus particle production has not been possible. Recently, an HCV cell culture system was developed using a genotype 2a strain, JFH-1, cloned from a fulminant hepatitis patient (14, 29, 32), thereby allowing investigation of the entire life cycle of this virus. However, several groups of investigators have reported genotype- and/or strain-dependent effects of some antiviral reagents (6, 17) and neutralizing antibodies (7, 25). Therefore, efficient virus production systems using various genotypes and strains are indispensable for HCV research and the development of antiviral strategies.

The JFH-1 strain is the first HCV strain that can efficiently produce HCV particles in HuH-7 cells (29). Other strains can replicate and produce infectious virus by HCV RNA transfection, but the efficiency is far lower than that of JFH-1 (24, 31). In the case of replication-incompetent strains, chimeric virus containing the JFH-1 nonstructural protein coding region is useful for analyses of viral characteristics (6, 9, 14, 23, 30, 31).

In this study, we developed a genotype 2b chimeric infectious virus production system using the MA strain (accession number AB030907) (19) harboring minimal regions of JFH-1 and cell culture-adaptive mutations that enhance infectious virus production.

MATERIALS AND METHODS

Cell culture. Huh7.5.1 cells (a kind gift from Francis V. Chisari) (32) and Huh7-25 cells (1) were cultured at 37°C in Dulbecco's modified Eagle's medium containing 10% fetal bovine serum under 5% CO_2 conditions. For follow-up study, RNA-transfected cells were passaged every 2 to 5 days depending on cell status.

Full-length genomic HCV constructs. Plasmids used in the analysis of genomic RNA replication were constructed based on pJFH1 (29) and pMA (19). For convenience, an EcoRI recognition site was introduced upstream of the T7 promoter region of pMA by PCR, and an XbaI recognition site was introduced at the end of the 3′ untranslated region (UTR). To construct MA/JFH-1, the EcoRI-BsaBI (nucleotides [nt] 1 to 2570; 5′ UTR to E2) fragment of pMA was substituted into pJFH1 (Fig. 1A). Replacement of the 5′ UTR was performed by exchanging the EcoRI-AgeI (nt 1 to 159) fragment. A point mutation in the core region (R167G) was introduced into MA chimeric constructs by PCR using the following primers: sense, 5′-TTA TGC AAC GGG GAA TTT ACC CGG TTG CTC T-3′; antisense, 5′-GGT AAA TTC CCC GTT GCA TAA TTT ATC CCG TC-3′. G167R substitution in the JFH-1 construct was performed by PCR using the following primers: sense, 5′-ATT ATG CAA CAA GGA ACC TAC CCG GTT TCC C-3′; antisense, 5′-GGT AGG TTC CTT GTT GCA TAA TTA ACC CCG TC-3′. Point mutations (L814S, R1012G, T1106A, and V1951A) were introduced into MA chimeric constructs by PCR using the following primers: L814S, 5′-GCT TAC GCC TCG GAC GCC GCT GAA CAA GGG G-3′ (sense) and 5′-AGC GGC GTC CGA GGC GTA AGC CTG CTG CGG C-3′ (antisense); R1012G, 5′-GAG GCT AGG TGG

Received 13 June 2011 Accepted 23 November 2011
Published ahead of print 7 December 2011
Address correspondence to Takaji Wakita, wakita@nih.go.jp.
* Present address: Institute of Microbial Chemistry, Shinagawa-ku, Tokyo, Japan.

doi:10.1128/JVI.05386-11

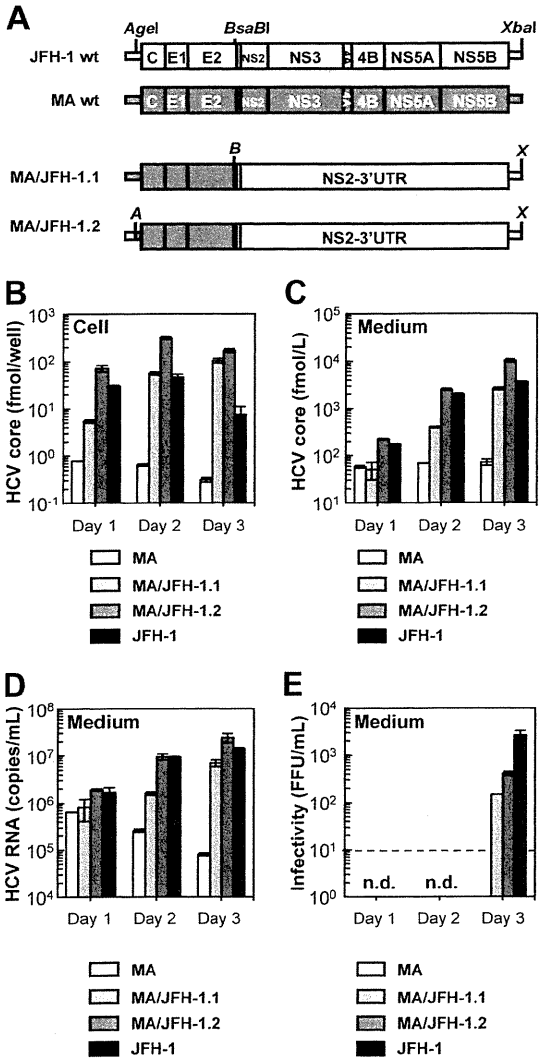

FIG 1 Replication and virus production by MA/JFH-1 chimeras in Huh7.5.1 cells. (A) Schematic structures of JFH-1, MA, and two MA/JFH-1 chimeras (MA/JFH-1.1 and MA/JFH-1.2). The junction of JFH-1 and MA in the 5′ UTR is an AgeI site, and the junction of MA and JFH-1 in the NS2 region is a BsaBI site. A, AgeI; B, BsaBI; X, XbaI. (B to E) Chimeric HCV RNA replication in Huh7.5.1 cells. HCV core protein level in cells (B) and culture medium (C) and HCV RNA levels in medium (D) and infectivity of culture medium (E) from HCV RNA-transfected Huh7.5.1 cells are shown. Ten micrograms of HCV RNA was transfected into Huh7.5.1 cells, and cells and culture medium were harvested on days 1, 2, and 3. n.d., not determined. Assays were performed three times independently, and data are presented as means ± standard deviation. Dashed line indicates detection limit. wt, wild type.

GGA AGT TCT GCT CGG CCC T-3′ (sense) and 5′-AGA ACT TCC CCA CCT AGC CTC GCG GAA ACC G-3′ (antisense); T1106A, 5′-CAG ATG TAC GCC AGC GCA GAG GGG GAC CTC-3′ (sense) and 5′-CTG CGC TGG CGT ACA TCT GGG TGA CTG GTC-3′ (antisense); and V1951A, 5′-GTG ACG CAG GCG TTA AGC TCA CTC ACA ATT ACC-3′ (sense) and 5′-TGA GCT TAA CGC CTG CGT CAC GCG CAG CGA G-3′ (antisense). To construct the MA chimeric virus harboring minimal regions of JFH-1 (MA/N3H+N5BX-JFH1), ClaI (nt 3930), EcoT22I (nt 5294), and BsrGI (nt 7782) recognition sites were introduced into pMA by site-directed mutagenesis. The 5′ UTR (EcoRI-AgeI), the region of the NS3 helicase (N3H; ClaI-EcoT22I), and the region of NS5B to 3′ X (N5BX; BsrGI-XbaI) were then replaced with the corresponding regions from JFH-1.

RNA synthesis, transfection, and determination of infectivity. RNA synthesis and transfection were performed as described previously (12, 22). Determination of infectivity was also performed as described previously, with infectivity expressed as the number of focus-forming units per milliliter (FFU/ml) (12, 22). When necessary, culture medium was concentrated 20-fold in Amicon Ultra-15 spin columns (100-kDa molecular-weight-cutoff; Millipore, Bedford, MA) in order to determine infectivity.

Quantification of HCV core protein and HCV RNA. In order to estimate the concentration of HCV core protein in culture medium, we performed a chemiluminescence enzyme immunoassay (Lumipulse II HCV core assay; Fujirebio, Tokyo, Japan) in accordance with the manufacturer's instructions. HCV RNA from harvested cells or culture medium was isolated using an RNeasy Mini RNA kit (Qiagen, Tokyo, Japan) or QiaAmp Viral RNA Minikit (Qiagen), respectively. Copy number of HCV RNA was determined by real-time quantitative reverse transcription-PCR (qRT-PCR), as described previously (28).

HCV sequencing. Total RNA in culture supernatant was extracted with Isogen-LS (Nippon Gene Co., Ltd., Tokyo, Japan). cDNA was synthesized using Superscript III Reverse Transcriptase (Invitrogen, Carlsbad, CA). cDNA was subsequently amplified with LA *Taq* DNA polymerase (TaKaRa, Shiga, Japan). Four separate PCR primer sets were used to amplify the fragments of nt 130 to 2909, 2558 to 5142, 4784 to 7279, and 7081 to 9634 covering the entire open reading frame and part of the 5′ UTR and 3′ UTR of the MA strain. Sequences of amplified fragments were determined directly.

Immunostaining. Infected cells were cultured on Multitest Slides (MP Biomedicals, Aurora, OH) and were fixed in acetone-methanol (1:1, vol/vol) for 15 min at −20°C. After a blocking step, infected cells were visualized with anti-core protein antibody (clone 2H9) (29) and Alexa Fluor 488 goat anti-mouse IgG (Invitrogen), and nuclei were visualized with 4′,6′-diamidino-2-phenylindole (DAPI).

Assessment of interferon sensitivity. Two micrograms of *in vitro* transcribed RNA was transfected into 3×10^6 Huh7.5.1 cells. Four hours after transfection, cells were placed in fresh medium or medium containing 0.1, 1, 10, 100, and 1,000 IU/ml of interferon α-2b (Intron A; Schering-Plough Corporation, Osaka, Japan). Culture medium was then harvested on day 3, and HCV core levels in the cells and in the medium were measured.

Statistical analysis. Significant differences were evaluated by Student's *t* test. A P value of <0.05 was considered significant.

RESULTS

Transient replication and production of 2b/2a chimeric virus. We first tested whether the MA strain (genotype 2b) (19) was able to replicate and produce infectious virus in cultured cells. When the *in vitro* transcribed RNA of MA was transfected into Huh7.5.1 cells, a highly HCV-permissive cell line, replication and virus production were not observed (Fig. 1A to C). We then tested whether 2b/2a chimeric RNA harboring the structural region (5′ UTR to E2) of the MA strain and the nonstructural region (p7 to 3′ UTR) of JFH-1 (Fig. 1A, MA/JFH-1.1) was able to replicate in the cells. After MA/JFH-1.1 RNA transfection, time-dependent accumulation of core protein in the cells (Fig. 1B) and culture medium (Fig. 1C) was observed, indicating that MA/JFH-1.1 RNA was able to replicate in the cells autonomously. HCV RNA levels in the medium were determined by qRT-PCR, and time-dependent increases in HCV RNA level were also observed (Fig. 1D). Infectious virus production was observed on day 3, but infectivity was 17.6-fold lower than that of JFH-1 (Fig. 1E).

In order to improve the level of infectious virus production, we tested another chimeric construct, MA/JFH-1.2, which contained an additional MA-to-JFH-1 replacement of the 5′ UTR (Fig. 1A),